Preprint typeset in JHEP style - HYPER VERSION FSU-HEP-050530

Mixed Wino Dark Matter: Consequences for Direct, Indirect and Collider Detection

Howard Baer, Azar Mustafayev, Eun-Kyung Park and Stefano Profumo

Department of Physics, Florida State University Tallahassee, FL 32306, USA
E-mail: baer@hep.fsu.edu,mazar@hep.fsu.edu,
epark@hep.fsu.edu,profumo@hep.fsu.edu

Abstract: In supersymmetric models with gravity-mediated SUSY breaking and gaugino mass unification, the predicted relic abundance of neutralinos usually exceeds the strict limits imposed by the WMAP collaboration. One way to obtain the correct relic abundance is to abandon gaugino mass universality and allow a mixed wino-bino lightest SUSY particle (LSP). The enhanced annihilation and scattering cross sections of mixed wino dark matter (MWDM) compared to bino dark matter lead to enhanced rates for direct dark matter detection, as well as for indirect detection at neutrino telescopes and for detection of dark matter annihilation products in the galactic halo. For collider experiments, MWDM leads to a reduced but significant mass gap between the lightest neutralinos so that $\widetilde{Z}_2$ two-body decay modes are usually closed. This means that dilepton mass edges– the starting point for cascade decay reconstruction at the CERN LHC– should be accessible over almost all of parameter space. Measurement of the $m_{\widetilde{Z}_2} - m_{\widetilde{Z}_1}$ mass gap at LHC plus various sparticle masses and cross sections as a function of beam polarization at the International Linear Collider (ILC) would pinpoint MWDM as the dominant component of dark matter in the universe.

Keywords: Supersymmetry Phenomenology, Supersymmetric Standard Model, Dark Matter.

1. Introduction

In supersymmetric models of particle physics, R-parity is often imposed to avoid too rapid proton decay which can be induced by superpotential terms which violate baryon and lepton number conservation. One of the byproducts of R-parity conservation is that the lightest supersymmetric particle is absolutely stable, making it a good candidate particle to make up the bulk of dark matter (DM) in the universe. In gravity-mediated SUSY breaking models, dark matter candidate particles include the lightest neutralino or the gravitino. Here we will focus on the lightest neutralino $\widetilde{Z}_1$[1]; recent results on TeV scale gravitino dark matter can be found in Ref. [2]. The relic density of neutralinos in supersymmetric models can be straightforwardly calculated by solving the Boltzmann equation for the neutralino number density[3]. The central part of the calculation is to evaluate the thermally averaged neutralino annihilation and co-annihilation cross section times velocity. The computation requires evaluating many thousands of Feynman diagrams. Several computer codes are now publicly[4, 5] available which evaluate the neutralino relic density $\Omega_{\widetilde{Z}_1}h^2$.

The dark matter density of the universe has recently been inferred from the WMAP collaboration based on precision fits to anisotropies in the cosmic microwave background radiation[6]. The WMAP collaboration result for the relic density of cold dark matter (CDM) is that

$$\Omega_{CDM}h^2 = 0.113 \pm 0.009. \tag{1.1}$$

This result imposes a tight constraint on supersymmetric models which contain a dark matter candidate[7].

Many analyses have been recently performed in the context of the paradigm minimal supergravity model[8] (mSUGRA), where the parameter space is given by m_0, $m_{1/2}$, A_0, $\tan\beta$ and $sign(\mu)$. The mSUGRA model assumes the minimal supersymmetric model (MSSM) is valid between the mass scales $Q = M_{GUT}$ and $Q = M_{SUSY}$. A common mass m_0 ($m_{1/2}$) ((A_0)) is assumed for all scalars (gauginos) ((trilinear soft breaking parameters)) at $Q = M_{GUT}$, while the bilinear soft term B is traded for $\tan\beta$, the ratio of Higgs vevs, via the requirement of radiative electroweak symmetry breaking (REWSB). REWSB also determines the magnitude, but not the sign, of the superpotential Higgs mass term μ. Weak scale couplings and soft parameters can be computed via renormalization group (RG) evolution from $Q = M_{GUT}$ to $Q = M_{weak}$. Once weak scale parameters are known, then sparticle masses and mixings may be computed, and the associated relic density of neutralinos can be determined.

In most of mSUGRA parameter space, the relic density $\Omega_{\widetilde{Z}_1}h^2$ turns out to be much larger than the WMAP value. Many analyses have found just several allowed regions of parameter space:

- The bulk region occurs at low values of m_0 and $m_{1/2}$[9]. In this region, neutralino annihilation is enhanced by t-channel exchange of relatively light sleptons. The bulk region, featured prominently in many early analyses of the relic density, has been squeezed from below by the LEP2 bound on the chargino mass $m_{\widetilde{W}_1} > 103.5$ GeV, and from above by the tight bound from WMAP.

- The stau co-annihilation region at low m_0 for almost any $m_{1/2}$ value where $m_{\tilde{\tau}_1} \simeq m_{\widetilde{Z}_1}$, so that $\tilde{\tau}_1 - \widetilde{Z}_1$ and $\tilde{\tau}_1^+\tilde{\tau}_1^-$ co-annihilation help to reduce the relic density[10].
- The hyperbolic branch/focus point (HB/FP) region at large $m_0 \sim$ several TeV, where μ becomes small, and neutralinos efficiently annihilate via their higgsino components[11]. This is the case of mixed higgsino dark matter (MHDM).
- The A-annihilation funnel occurs at large $\tan\beta$ values when $2m_{\widetilde{Z}_1} \sim m_A$ and neutralinos can efficiently annihilate through the broad A and H Higgs resonances[12].

In addition, a less prominent light Higgs h annihilation corridor occurs at low $m_{1/2}$[13] and a top squark co-annihilation region occurs at particular A_0 values when $m_{\tilde{t}_1} \simeq m_{\widetilde{Z}_1}$[14].

Many analyses have also been performed for gravity-mediated SUSY breaking models with non-universal soft terms. Non-universality of SSB scalar masses can 1. pull various scalar masses to low values so that "bulk" annihilation via t-channel exchange of light scalars can occur[15], or 2. they can bring in new near degeneracies of various sparticles with the $\widetilde{Z}_1$ so that new co-annihilation regions open up[16, 17, 18], or they can 3. bring the value of m_A into accord with $2m_{\widetilde{Z}_1}$ so that funnel annihilation can occur[19, 17], or 4. they can pull the value of μ down so that higgsino annihilation can occur[19, 20, 17]. It is worthwhile noting that all these general mechanisms for increasing the neutralino annihilation rate already occur in the mSUGRA model. Moreover, in all these cases the lightest neutralino is either bino-like, or a bino-higgsino mixture.

If non-universal gaugino masses are allowed, then a qualitatively new possibility arises that is not realized in the mSUGRA model: that of mixed wino dark matter (MWDM). In this case, if the $SU(2)$ gaugino mass M_2 is sufficiently low compared to $U(1)_Y$ gaugino mass M_1, then the $\widetilde{Z}_1$ can become increasingly wino-like. The $\widetilde{Z}_1 - \widetilde{W}_{1,2} - W$ coupling becomes large when $\widetilde{Z}_1$ becomes wino-like, resulting in enhanced $\widetilde{Z}_1\widetilde{Z}_1 \to W^+W^-$ annihilations. Moreover, coannihilations with the lightest chargino and with the next-to-lightest neutralino help to further suppress the LSP thermal relic abundance.

Non-universal gaugino masses can arise in supersymmetric models in a number of ways[21].

- In supergravity GUT models, the gauge kinetic function (GKF) f_{AB} must transform as the symmetric product of two adjoints. In minimal supergravity, the GKF transforms as a singlet. In $SU(5)$ SUGRA-GUT models, it can also transform as a 24, 75 or 200 dimensional representation[22], while in $SO(10)$ models it can transform as 1, 54, 210 and 770 dimensional representations[23, 24]. Each of these non-singlet cases leads to unique predictions for the ratios of GUT scale gaugino masses. Furthermore, if the GKF transforms as a linear combination of these higher dimensional representations, then essentially arbitrary gaugino masses are allowed.
- Non-universal gaugino masses are endemic to heterotic superstring models with orbifold compactification where SUSY breaking is dominated by the moduli fields[25].
- Additionally, in extra-dimensional SUSY GUT models where SUSY breaking is communicated from the SUSY breaking brane to the visible brane via gaugino mediation,

various patterns of GUT scale gaugino masses can occur, including the case of completely independent gaugino masses[26].

In this report, we will adopt a phenomenological approach, and regard the three MSSM gaugino masses as independent parameters, with the constraint that the neutralino relic density should match the WMAP measured value.

Much previous work has been done on evaluating the relic density in models with gaugino mass non-universality. In AMSB models[27], the $\widetilde{Z}_1$ is almost pure wino, so that $\Omega_{\widetilde{Z}_1}h^2$ as predicted by the Boltzmann equation is typically very low. Moroi and Randall[28] proposed moduli decay to wino-like neutralinos in the early universe to account for the dark matter density. Already in 1991, Griest and Roszkowski had shown that a wide range of relic density values could be obtained by abandoning gaugino mass universality[29]. Corsetti and Nath investigated dark matter relic density and detection rates in models with non-minimal $SU(5)$ GKF and also in O-II string models[30]. Birkedal-Hanson and Nelson showed that a GUT scale ratio $M_1/M_2 \sim 1.5$ would bring the relic density into accord with the measured CDM density via MWDM, and also presented direct detection rates[31]. Bertin, Nezri and Orloff showed variation of relic density and enhancement in direct and indirect DM detection rates as non-universal gaugino masses were varied[32]. Bottino *et al.* performed scans over independent weak scale parameters to show variation in indirect DM detection rates, and noted that neutralinos as low as 6 GeV are allowed[33]. Belanger *et al.* presented relic density plots in the m_0 $vs.m_{1/2}$ plane for a variety of universal and non-universal gaugino mass scenarios, and showed that large swaths of parameter space open up when the $SU(3)$ gaugino mass M_3 becomes small[34]. Mambrini and Munoz and also Cerdeno and Munoz showed direct and indirect detection rates for model with scalar and gaugino mass non-universality[35]. Auto *et al.*[16] used non-universal gaugino masses to reconcile the predicted relic density in models with Yukawa coupling unification with the WMAP result. Masiero, Profumo and Ullio exhibit the relic density and direct and indirect detection rates in split supersymmetry where M_1, M_2 and μ are taken as independent weak scale parameters with ultra-heavy squarks and sleptons[36].

In this paper, we will adopt a model with GUT scale parameters including universal scalar masses, but with independent gaugino masses leading to MWDM. We will assume all gaugino masses to be of the same sign. The opposite sign situation leads to a distinct DM scenario and will be addressed soon[37]. We will adjust the gaugino masses such that $\widetilde{Z}_1$ receives just enough of a wino component so that it makes up the entire CDM density as determined by WMAP without the need for late-decaying moduli fields. In fact, the wino component of the $\widetilde{Z}_1$ is usually of order $0.1-0.2$, so that the $\widetilde{Z}_1$ is still mainly bino-like, but with a sufficiently large admixture of wino as to match the WMAP result on $\Omega_{CDM}h^2$. In Sec. 2, we present the parameter space for MWDM, and show how the assumption of MWDM influences the spectrum of sparticle masses. In Sec. 3, we show rates for direct and indirect detection of MWDM. These rates are usually enhanced relative to mSUGRA due to the enhanced wino component of the $\widetilde{Z}_1$. In Sec. 4, we investigate consequences of MWDM for the CERN LHC and the international linear e^+e^- collider (ILC). The goal here is to devise a set of measurements that can differentiate MWDM

from the usual case of bino-like DM or MHDM as expected in the mSUGRA model. For MWDM, the neutralino mass gap $m_{\widetilde{Z}_2} - m_{\widetilde{Z}_1}$ is almost always less than M_Z, so that two-body decays of $\widetilde{Z}_2$ are closed, and three body decays are dominant. The $m_{\widetilde{Z}_2} - m_{\widetilde{Z}_1}$ mass gap is directly measurable at the CERN LHC via the well-known edge in the $m(\ell^+\ell^-)$ distribution. The correlation of the $\widetilde{Z}_2 - \widetilde{Z}_1$ mass gap against direct and indirect detection rates provides a distinction between the possible DM candidates. Measurements of the $m_{\widetilde{Z}_2} - m_{\widetilde{Z}_1}$ mass gap at the LHC combined with measurements of chargino and neutralino masses and production cross sections as a function of beam polarization at the ILC would provide the ultimate determination of the presence of MWDM in the universe. In Sec. 5, we present our conclusions.

2. Relic density and sparticle mass spectrum

Our goal is to explore SUGRA models with non-universal gaugino masses leading to MWDM with a neutralino relic density in accord with the WMAP result. To do so, we adopt the subprogram Isasugra, which is a part of the Isajet 7.72 event generator program[38]. Isasugra allows supersymmetric spectra generation using a variety of GUT scale non-universal soft SUSY breaking terms. The Isasugra spectrum is generated using 2-loop MSSM RGEs for coupling and soft SUSY breaking term evolution. An iterative approach is used to evaluate the supersymmetric spectrum. Electroweak symmetry is broken radiatively, so that the magnitude, but not the sign, of the superpotential μ parameter is determined. The RG-improved 1-loop effective potential is minimized at an optimized scale which accounts for leading 2-loop terms. Full 1-loop radiative corrections are incorporated for all sparticle masses. To evaluate the neutralino relic density, we adopt the IsaReD program[5], which is based on CompHEP to compute the several thousands of neutralino annihilation and co-annihilation Feynman diagrams. Relativistic thermal averaging of the cross section times velocity is performed[39]. The parameter space we consider is given by

$$m_0,\ m_{1/2},\ A_0,\ \tan\beta,\ sign(\mu),\ M_1 \text{ or } M_2, \tag{2.1}$$

where we take either M_1 or M_2 to be free parameters, and in general not equal to $m_{1/2}$.

In Fig. 1, we show our first result. Here, we take $m_0 = m_{1/2} = 300$ GeV, with $A_0 = 0$, $\tan\beta = 10$, $\mu > 0$ with $m_t = 178$ GeV. We plot the neutralino relic density $\Omega_{\widetilde{Z}_1}h^2$ in frame *a*) versus variation in the $U(1)$ gaugino mass M_1. At $M_1 = 300$ GeV, we are in the mSUGRA case, and $\Omega_{\widetilde{Z}_1}h^2 = 1.3$, so that the model would be excluded by WMAP. By decreasing M_1, the bino-like neutralino becomes lighter until two dips in the relic density occur. These correspond to the cases where $2m_{\widetilde{Z}_1} \simeq m_h$ and M_Z as one moves towards decreasing M_1, *i.e.* one has either light Higgs h or Z resonance annihilation. As M_1 increases past its mSUGRA value, the $\widetilde{Z}_1$ becomes increasing wino-like, and the relic density decreases. The $W - \widetilde{W}_{1,2} - \widetilde{Z}_1$ coupling is proportional to the $SU(2)_L$ gaugino component of the neutralino, (and also to the Higgsino components), and so $\widetilde{Z}_1\widetilde{Z}_1 \to W^+W^-$ annihilation becomes enhanced, and the relic density is lowered. In this case, the WMAP $\Omega_{\widetilde{Z}_1}h^2$ value is reached for $M_1 = 490$ GeV. For still higher M_1 values,

$\Omega_{\widetilde{Z}_1}h^2$ drops precipitously, so that other non-neutralino dark matter candidates would have to exist to account for the dark matter density in the universe. In frame *b*), we show the bino/wino fraction $R_{\widetilde{B},\widetilde{W}}$ of the $\widetilde{Z}_1$. Here, we adopt the notation of Ref. [40], wherein the lightest neutralino is written in terms of its (four component Majorana) Higgsino and gaugino components as

$$\widetilde{Z}_1 = v_1^{(1)}\psi_{h_u^0} + v_2^{(1)}\psi_{h_d^0} + v_3^{(1)}\lambda_3 + v_4^{(1)}\lambda_0, \tag{2.2}$$

where $R_{\widetilde{W}} = |v_3^{(1)}|$ and $R_{\widetilde{B}} = |v_4^{(1)}|$. While $R_{\widetilde{W}}$ increases as M_1 increases, its value when $\Omega_{\widetilde{Z}_1}h^2$ reaches the WMAP value is still only ~ 0.25, while $R_{\widetilde{B}} \sim 0.9$. Thus, the $\widetilde{Z}_1$ is still mainly bino-like, with just enough admixture of wino to give the correct relic density. This corresponds to the case of MWDM. A similar plot is obtained by lowering M_2, rather than raising M_1, as shown in Fig. 2.

By raising or lowering the GUT scale gaugino masses in SUGRA models, the mass of the neutralinos will obviously change since M_1 and M_2 enter directly into the neutralino mass matrix. However, various other sparticle masses will also be affected by varying the gaugino masses, since these feed into the soft term evolution via the RGEs. In Fig. 3, we show the variation of the sparticle mass spectrum with respect to the GUT scale ratio $M_1/m_{1/2}$ for the same parameters as in Fig. 1. When $M_1/m_{1/2} = 1$, there is a relatively large mass gap between $\widetilde{Z}_2$ and $\widetilde{Z}_1$: $m_{\widetilde{Z}_2} - m_{\widetilde{Z}_1} = 106.7$ GeV. As M_1 is increased until $\Omega_{\widetilde{Z}_1}h^2 = 0.11$, the mass gap shrinks to $m_{\widetilde{Z}_2} - m_{\widetilde{Z}_1} = 31.9$ GeV. The light chargino mass $m_{\widetilde{W}_1}$ remains essentially constant in this case, since M_2 remains fixed at 300 GeV. However, we notice that as M_1 increases, the $\tilde{e}_R$, $\tilde{\mu}_R$ and $\tilde{\tau}_1$ masses also increase, since M_1 feeds into their mass evolution via RGEs. As the coefficient appearing in front of M_1 in the RGEs is larger (and with the same sign) for the right handed sfermions than for the left handed ones, one expects, in general, a departure from the usual mSUGRA situation where the lightest sleptons are right-handed. As a matter of fact, whereas in mSUGRA $m_{\tilde{e}_L} >> m_{\tilde{e}_R}$, in the case of MWDM, instead, for the particular parameter space slice under consideration, we

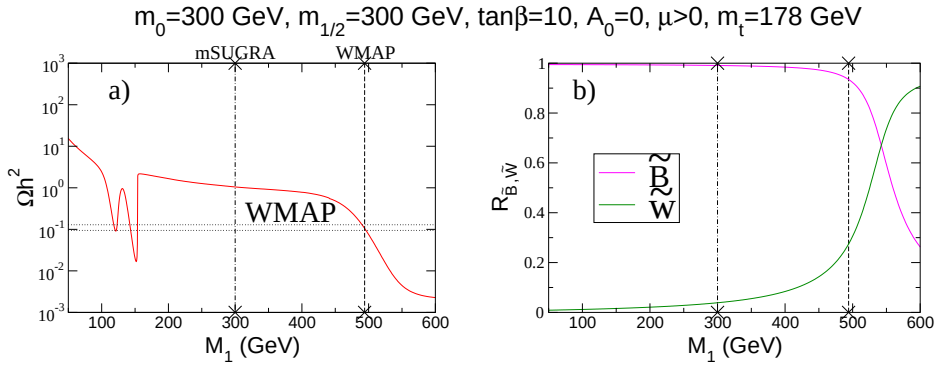

Figure 1: A plot of *a*) relic density $\Omega_{CDM}h^2$ and *b*) bino/wino component of the lightest neutralino as a function of M_1 for $m_0 = 300$ GeV, $m_{1/2} = 300$ GeV, $A_0 = 0$, $\tan\beta = 10$, $\mu > 0$ and $m_t = 178$ GeV.

find that $m_{\tilde{e}_L} \sim m_{\tilde{e}_R}$. As shown in the figure, the right-handed squark masses also increase with increasing M_1, although the relative effect is less dramatic than the case involving sleptons: the dominant driving term in the RGEs is, in this case, given by M_3 (absent in the case of sleptons), hence variations in the GUT value of M_1 produce milder effects.

In Fig. 4, we show a plot of sparticle masses for the same parameters as in Fig. 3, but versus $M_2/m_{1/2}$. In this case, as M_2 is decreased from its mSUGRA value of 300 GeV, the $\widetilde{W}_1$ and $\widetilde{Z}_2$ masses decrease until $\Omega_{\widetilde{Z}_1}h^2$ reaches 0.11, where now $m_{\widetilde{Z}_2} - m_{\widetilde{Z}_1} = 22.9$ GeV. In this case, with decreasing M_2, the left- slepton and sneutrino masses also decrease, again leading to $m_{\tilde{e}_L} \sim m_{\tilde{e}_R}$. The left-handed squark masses similarly decrease. Right-handed sfermion masses are, instead, not affected, with the net result that the mSUGRA $m_{\tilde{e}_L} >> m_{\tilde{e}_R}$ hierarchy is again altered.

The effect of varying gaugino masses on the allowed region of parameter space is illustrated in Fig. 5. Here, in frame *a*), we show the case of the mSUGRA model in the m_0 *vs.* $m_{1/2}$ plane for $A_0 = 0$, $\tan\beta = 10$ and $\mu > 0$. The red shaded regions are disallowed by either a stau LSP (left side of plot) or lack of REWSB (lower edge of plot). The blue shaded region has a chargino with mass $m_{\widetilde{W}_1} < 103.5$ GeV, thus violating bounds from LEP2. The dark green shaded region has $0.094 < \Omega_{\widetilde{Z}_1}h^2 < 0.129$, in accord with the WMAP measurement. The light green shaded region has $\Omega_{\widetilde{Z}_1}h^2 < 0.094$, so that additional sources of dark matter would be needed. We see the stau co-annihilation region appearing along the left edge of the allowed parameter space, and the bulk region appearing at low m_0 and low $m_{1/2}$. The h annihilation corridor appears also at low $m_{1/2}$ along the edge of the LEP2 excluded region. In frame *b*), we take $M_1/m_{1/2} = 1.5$, so that the $\widetilde{Z}_1$ becomes more wino-like. In response, we see that a large new bulk region has appeared at low m_0 and low $m_{1/2}$. In frame *c*), we increase $M_1/m_{1/2}$ to 1.75. In this case, most of the m_0 *vs.* $m_{1/2}$ plane is now allowed, although much of it has $\Omega_{\widetilde{Z}_1}h^2$ below the WMAP central value for the CDM relic density.

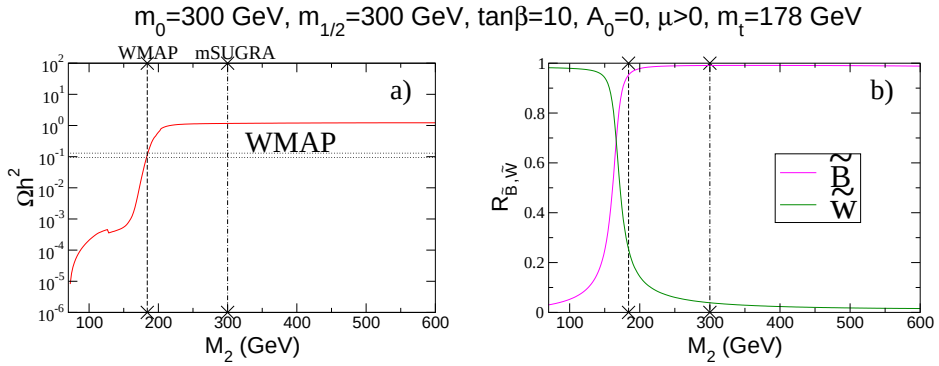

Figure 2: A plot of *a*) relic density $\Omega_{CDM}h^2$ and *b*) bino/wino component of the lightest neutralino as a function of M_2 for $m_0 = 300$ GeV, $m_{1/2} = 300$ GeV, $A_0 = 0$, $\tan\beta = 10$, $\mu > 0$ and $m_t = 178$ GeV.

It should be apparent now that *any* point in the m_0 *vs.* $m_{1/2}$ plane can become WMAP allowed by either increasing M_1 or decreasing M_2 to a suitable degree as to obtain MWDM. To illustrate this, we plot in Fig. 6 the ratio $r_1 \equiv M_1/m_{1/2}$ in frame *a*) or $r_2 = M_2/m_{1/2}$ in frame *b*) needed to achieve a relic density in accord with the WMAP central value. We see in frame *a*) that r_1 increases as one moves from lower-left to upper-right, reflecting the greater wino component of $\widetilde{Z}_1$ that is needed to overcome the increasing $\Omega_{\widetilde{Z}_1}h^2$ which is expected in the mSUGRA model. We also see on the left side of the plot that $r_1 \leq 1$ is allowed, since then $\Omega_{\widetilde{Z}_1}h^2 \leq 0.11$ already in the mSUGRA case. The structure at high $m_{1/2}$ and $m_0 \sim 400 - 500$ GeV results because increasing M_1 increases $m_{\widetilde{Z}_1}$ until $2m_{\widetilde{Z}_1} \sim m_A$ and the A-funnel begins to come into effect (even though $\tan\beta$ is small).

3. Direct and indirect detection of mixed wino dark matter

In this section, we turn to consequences of MWDM for direct and indirect detection of neutralino dark matter[41, 42]. We adopt the DarkSUSY code[43], interfaced to Isajet, for the computation of the various rates, and resort to the Adiabatically Contracted N03 Halo model[44] for the dark matter distribution in the Milky Way[1]. We evaluate the following neutralino DM detection rates:

- Direct neutralino detection via underground cryogenic detectors[48]. Here, we compute the spin independent neutralino-proton scattering cross section, and compare it to expected sensitivities[49] for Stage 2 detectors (CDMS2[50], Edelweiss2[51], CRESST2[52], ZEPLIN2[53]) and for Stage 3, ton-size detectors (XENON[54], Genius[55], ZEPLIN4[56] and WARP[57]). We take here as benchmark experimental reaches of Stage 2 and Stage 3 detectors the projected sensitivities of, respectively, CDMS2 and XENON 1-ton at the corresponding neutralino mass.

- Indirect detection of neutralinos via neutralino annihilation to neutrinos in the core of the Sun[58]. Here, we present rates for detection of $\nu_\mu \to \mu$ conversions at Antares[59] or IceCube[60]. The reference experimental sensitivity we use is that of IceCube, with a muon energy threshold of 25 GeV, corresponding to a flux of about 40 muons per km^2 per year.

- Indirect detection of neutralinos via neutralino annihilations in the galactic center leading to gamma rays[61], as searched for by EGRET[62], and in the future by GLAST[63]. We evaluate the integrated continuum γ ray flux above a $E_\gamma = 1$ GeV threshold, and assume a GLAST sensitivity of 1.0×10^{-10} cm^{-2}s^{-1}.

- Indirect detection of neutralinos via neutralino annihilations in the galactic halo leading to cosmic antiparticles, including positrons[64] (HEAT[65], Pamela[66] and AMS-02[67]), antiprotons[68] (BESS[69], Pamela, AMS-02) and anti-deuterons ($\bar{D}$s) (BESS[70], AMS-02, GAPS[71]). For positrons and antiprotons we evaluate the averaged differential antiparticles flux in a projected energy bin centered at a kinetic

[1]For a comparison of the implications of different halo model choices for indirect DM detection rates, see *e.g.* Refs. [45, 46, 47, 17].

energy of 20 GeV, where we expect an optimal statistics and signal-to-background ratio at space-borne antiparticles detectors[47, 72]. We use as benchmark experimental sensitivity that of the Pamela experiment after three years of data-taking. Finally, the average differential antideuteron flux has been computed in the $0.1 < E_{\bar{D}} < 0.4$ GeV range, and compared to the estimated GAPS sensitivity[71].

In Fig. 7, we show various direct and indirect DM detection rates for $m_0 = m_{1/2} = 300$ Gev, with $A_0 = 0$, $\tan\beta = 10$ and $\mu > 0$, while M_1 is allowed to vary. The M_1 value corresponding to the mSUGRA model is denoted by a dot-dashed vertical line, while the one where $\Omega_{\widetilde{Z}_1} h^2 = 0.11$ by a dashed vertical line denoted WMAP.

In frame *a*), we plot the spin-independent neutralino-proton scattering cross section. Both the squark-mediated and Higgs mediated neutralino-proton scattering amplitudes are enhanced by more than one order of magnitude due to the increasing wino nature of the $\widetilde{Z}_1$. The reason for the enhancement is traced back to the structure of the neutralino-quark-squark and neutralino-neutralino-Higgs couplings, where the wino fraction is weighed by the $SU(2)$ coupling, while the bino fraction by the (smaller) $U(1)$ coupling.

In frame *b*), we show the flux of muons from neutralino pair annihilations in the core of the Sun. While the muon flux is below the reach of IceCube in the mSUGRA case, it has climbed into the observable region when the $\widetilde{Z}_1$ has become sufficiently wino-like as to fulfill the WMAP measured DM relic density.

In frames *c*), *d*), *e*) and *f*) we show the flux of photons, positrons, antiprotons and antideuterons, respectively. The results here are plotted as ratios of fluxes normalized to the mSUGRA point, in order to give results that are approximately halo-model independent. (We do show the above described expected experimental reach lines as obtained by using the Adiabatically Contracted N03 Halo model[44].) All rates are enhanced, with respect to the mSUGRA case, by 2 to 3 orders of magnitude, due to the increasing cross section for $\widetilde{Z}_1\widetilde{Z}_1 \to W^+W^-$ annihilation in the galactic halo. In particular, antimatter fluxes are always below future sensitivities for the mSUGRA setup, while they all rise to a detectable level when the WMAP point is reached.

In Fig. 8, we show the same direct and indirect DM detection rates as in Fig. 7, except this time versus M_2 instead of M_1. In this case, the various rates are all increasing as M_2 decreases, entering the region of MWDM. Indirect detection rates again feature enhancements as large as 2 orders of magnitude with respect to the mSUGRA scenario, when the WMAP relic abundance is reached. The abrupt decrease in the rates below $M_2 \sim 100$ GeV is due, instead, to the $m_{\widetilde{Z}_1} < m_W$ threshold.

In Fig. 9, we show regions of the m_0 *vs.* $m_{1/2}$ plane for $A_0 = 0$, $\tan\beta = 10$ and $\mu > 0$ which are accessible to various direct and indirect DM search experiments. The visibility criteria we adopt here follow the same approach outlined in Ref. [17]. The gray shaded regions in the plots are already excluded, at 95% C.L., by a χ^2 analysis of the computed signal plus background $\bar{p}$ flux compared to the available antiprotons data (for details see[47]). Observable rates for γ detection by GLAST occur throughout all three planes, due to the high DM density assumed at the galactic core in the N03 halo model. In frame *a*), we show the case of the mSUGRA model. Only small regions at low m_0

and low $m_{1/2}$ are accessible to $\bar{D}$ searches by GAPS and $\bar{p}$ searches by Pamela. A tiny region is also accessible to CDMS2, and a much larger region is accessible to Stage 3 direct detection experiments such as XENON. In frame *b*), we increase $M_1(M_{GUT})$ at every point in the plane as in Fig. 6 until $\Omega_{\widetilde{Z}_1}h^2 = 0.11$. The corresponding neutralino masses are therefore accordingly increased with respect to the mSUGRA case. Nevertheless, we see that the regions accessible to direct and indirect DM detection have vastly increased. The $\bar{D}$ search by GAPS can cover $m_{1/2} \lesssim 400 - 500$ GeV. The e^+ and $\bar{p}$ searches by Pamela can see to $m_{1/2} \sim 250$ GeV and 350 GeV, respectively. In addition, a region has opened up which is accessible to IceCube searches for dark matter annihilation in the core of the Sun. The Stage 3 dark matter detectors can see most of the m_0 *vs.* $m_{1/2}$ plane, with the exception of the region at large $m_{1/2}$ and low m_0 where a much lower wino component of the $\widetilde{Z}_1$ is required to bring the relic density into line with the WMAP measurement (here, early universe $\widetilde{Z}_1\widetilde{Z}_1$ annihilations are already somewhat enhanced by the proximity of the A-pole and the stau co-annihilation region). In frame *c*), we show again the m_0 *vs.* $m_{1/2}$ plane, but this time we have *reduced* M_2 until the $\Omega_{\widetilde{Z}_1}h^2 = 0.11$ value is reached. Again, many of the direct and indirect detection regions are expanded compared to the mSUGRA case. We remark that, although in this last case the neutralino mass is lower than in the case shown in frame *b*), direct detection and neutrino fluxes are somewhat less favored. This depends on the relative higgsino fraction, which critically enters in the neutralino-proton scattering cross section as well as in the neutralino capture rate in the Sun: raising M_1 shifts the gaugino masses closer to μ, hence increasing the higgsino fraction and the resulting neutralino cross sections off matter.

4. Mixed wino dark matter at colliders

An important question is whether collider experiments would be able to distinguish the case of MWDM from other forms of neutralino DM such as bino-DM or MHDM as occur in the mSUGRA model. We have seen from the plots of sparticle mass spectra that the squark and gluino masses vary only slightly with changing M_1 or M_2. However, the chargino and neutralino masses change quite a bit, and in fact rather small mass gaps $m_{\widetilde{W}_1} - m_{\widetilde{Z}_1}$ and $m_{\widetilde{Z}_2} - m_{\widetilde{Z}_1}$ are in general expected in the case of MWDM as compared with the case from models containing gaugino mass unification.

In Fig. 10, we show contours of the mass gap $m_{\widetilde{Z}_2} - m_{\widetilde{Z}_1}$ in the m_0 *vs.* $m_{1/2}$ plane for $A_0 = 0$, $\tan\beta = 10$ and $\mu > 0$ for *a*) the mSUGRA model, *b*) the case of MWDM where M_1 is raised at every point until $\Omega_{\widetilde{Z}_1}h^2 \to 0.11$ and *c*) the case of MWDM where M_2 is lowered until $\Omega_{\widetilde{Z}_1}h^2 \to 0.11$. In the case of the mSUGRA model, most of the parameter space has $m_{\widetilde{Z}_2} - m_{\widetilde{Z}_1} > 90$ GeV, which means that $\widetilde{Z}_2 \to \widetilde{Z}_1 Z^0$ decay is allowed. When this decay is allowed, its branching fraction is always large, unless it competes with other two-body decays such as $\widetilde{Z}_2 \to \widetilde{Z}_1 h$ or $\widetilde{Z}_2 \to \bar{f}\tilde{f}$ or $f\bar{\tilde{f}}$ (where f is a SM fermion). In the case of MWDM in frames *b*) and *c*), we see that (aside from the left-most portion of frame *b*), which is not a region of MWDM), the mass gap is much smaller, so that two-body decays of $\widetilde{Z}_2$ and $\widetilde{W}_1$ are closed and three-body decays are dominant.

When the decays $\widetilde{Z}_2 \to \tilde{\ell}\bar{\ell}$, $\bar{\tilde{\ell}}\ell \to \widetilde{Z}_1\ell\bar{\ell}$ or $\widetilde{Z}_2 \to \widetilde{Z}_1\ell\bar{\ell}$ are open ($\ell = e$ or μ), then prospects are good for measuring the $\widetilde{Z}_2 - \widetilde{Z}_1$ mass gap at the CERN LHC and possibly at the Fermilab Tevatron. If $\widetilde{Z}_2$'s are produced at large rates either directly or via gluino or squark cascade decays[73], it should be possible to identify opposite sign/ same flavor dilepton pairs, to reconstruct their invariant mass, and extract the upper edge of the invariant mass distribution[74]. In Fig. 11, we show the branching fraction $BF(\widetilde{Z}_2 \to \widetilde{Z}_1 e^+e^-)$ versus M_1 (left-side) or versus M_2 (right-side) for a variety of choices of m_0, $m_{1/2}$ and $\tan\beta$. The mSUGRA model value is denoted by the dot-dashed vertical line, while the $M_{1,2}$ value at which $\Omega_{\widetilde{Z}_1}h^2 \to 0.11$ is indicated by the dotted vertical line. As one moves to higher M_1 (or lower M_2) values, in most cases the leptonic three-body decays of $\widetilde{Z}_2$ become enhanced, usually because as M_1 grows (M_2 decreases), the two-body decay modes become kinematically closed, and only three-body decays are allowed. Thus, while the mSUGRA model yields large rates for $\widetilde{Z}_2 \to \widetilde{Z}_1 e^+e^-$ only when $m_{1/2} \lesssim 220$ GeV, this decay mode is almost always open in the case of MWDM. The only exception occurs when the stau co-annihilation or the A-funnel act to lower the relic density, so that a large M_1 or small M_2 is not needed to obtain the correct relic density; this, however, is not the case of MWDM.

4.1 CERN LHC

If the R-parity conserving MSSM is a good description of nature at the weak scale, then multi-jet plus multi-lepton plus $\not{E}_T$ events should occur at large rates at the CERN LHC, provided that $m_{\tilde{g}} \lesssim 2-3$ TeV. The LHC reach for SUSY in the mSUGRA model has been calculated in Ref. [75]. The mSUGRA reach results should also apply qualitatively to the MWDM case, since the values of $m_{\tilde{g}}$ and $m_{\tilde{q}}$ change little in going from mSUGRA to MWDM, and the reach plots mainly depend on these masses.

For SUSY searches at the CERN LHC, Hinchliffe *et al.* have pointed out[76] that an approximate value of $m_{\tilde{q}}$ or $m_{\tilde{g}}$ can be gained by extracting the maximum in the M_{eff} distribution, where $M_{eff} = \not{E}_T + E_T(jet\ 1) + E_T(jet\ 2) + E_T(jet\ 3) + E_T(jet\ 4)$. This statement holds true in models with MWDM, as well as in models with gaugino mass unification, so that the approximate mass scale of strongly interacting sparticles will be known soon after a supersymmetry signal has been established.

In mSUGRA, a dilepton mass edge should be visible in SUSY signal events only if $m_{1/2} \lesssim 250$ GeV or if $\widetilde{Z}_2 \to \tilde{\ell}\bar{\ell}$, $\bar{\tilde{\ell}}\ell$ decays are allowed. In the case of MWDM, the dilepton mass edge should be visible over almost all parameter space. We illustrate the situation for four case studies listed in Table 1. The first case, labeled mSUGRA, has $m_0 = m_{1/2} = 300$ GeV, with $A_0 = 0$, $\tan\beta = 10$ and $\mu > 0$. In this case, $\tilde{g}\tilde{g}$, $\tilde{g}\tilde{q}$ and $\tilde{q}\tilde{q}$ production occurs with a combined cross section of about 12 pb, while the total SUSY cross section is around 13.4 pb (the additional 1.4 pb comes mainly from -ino pair production and -ino-squark or -ino-gluino associated production). The case of MWDM1, with $M_1 = 490$ GeV, has similar rates of sparticle pair production. The case of MWDM2, with lighter chargino and neutralino masses, has a total production cross section of 19.2 pb, wherein strongly interacting sparticles are pair produced at similar rates as in mSUGRA or MWDM1, but -ino pairs are produced at a much larger rate ~ 6.1 pb. We also show a case of MHDM

parameter	mSUGRA	MWDM1	MWDM2	MHDM
M_1	300	490	300	300
M_2	300	300	187	300
μ	409.2	410.1	417.8	166.1
$m_{\tilde{g}}$	732.9	732.8	733.0	854.6
$m_{\tilde{u}_L}$	720.9	721.1	706.9	3467.2
$m_{\tilde{t}_1}$	523.4	526.0	533.2	2075.8
$m_{\tilde{b}_1}$	650.0	648.9	640.2	2847.0
$m_{\tilde{e}_L}$	364.7	371.7	330.0	3449.7
$m_{\tilde{e}_R}$	322.8	353.7	322.7	3449.4
$m_{\widetilde{W}_2}$	432.9	433.8	435.9	288.9
$m_{\widetilde{W}_1}$	223.9	224.0	138.3	146.6
$m_{\widetilde{Z}_4}$	433.7	435.7	436.2	296.9
$m_{\widetilde{Z}_3}$	414.8	415.6	424.1	179.0
$m_{\widetilde{Z}_2}$	223.7	225.4	138.8	159.2
$m_{\widetilde{Z}_1}$	117.0	193.5	115.9	101.5
m_A	538.6	544.1	523.6	3409.9
m_{H^+}	548.0	553.5	533.1	3433.3
m_h	115.7	115.8	115.3	118.9
$\Omega_{\widetilde{Z}_1}h^2$	1.3	0.11	0.11	0.13
$BF(b\to s\gamma)$	3.2×10^{-4}	3.2×10^{-4}	3.3×10^{-4}	3.4×10^{-4}
Δa_μ	12.1×10^{-10}	11.8×10^{-10}	15.9×10^{-10}	3.9×10^{-11}
$\sigma_{sc}(\widetilde{Z}_1 p)$	2.6×10^{-8} pb	2.2×10^{-7} pb	7.1×10^{-8} pb	1.8×10^{-8} pb

Table 1: Masses and parameters in GeV units for mSUGRA, MWDM and MHDM models. In the first three cases, $m_0 = m_{1/2} = 300$ GeV, $A_0 = 0$, $\tan\beta = 10$ and $m_t = 178$ GeV. The case of MHDM has the same parameters, except $m_0 = 3451.8$ GeV, with $m_t = 175$ GeV.

from the HB/FP region of the mSUGRA model as an alternative low $\widetilde{Z}_2 - \widetilde{Z}_1$ mass gap model to compare against MWDM scenarios.

We have generated 50K LHC SUSY events for each of these cases using Isajet 7.72, and passed them through a toy detector simulation. The toy detector is divided into calorimeter cells of size $\Delta\eta \times \Delta\phi = 0.05 \times 0.05$ extending out to $|\eta| < 5$, with no transverse shower spreading. We invoke EM smearing with $3\%/\sqrt{E}+.5\%$, hadronic smearing with $80\%/\sqrt{E}+3\%$ out to $|\eta| = 2.6$, and forward calorimeter hadronic smearing with $100\%/\sqrt{E}+5\%$. Jets are clustered using a UA1 type algorithm with cone size $R = \sqrt{\Delta\eta^2 + \Delta\phi^2} = 0.7$, with $E_{jet}(min) = 25$ GeV. Leptons ($\ell = e$ or μ) with $E_\ell > 10$ GeV are classified as isolated if $E_T(cone) < 5$ GeV in a cone of $R = 0.3$ about the lepton's direction. Since gluino and squark masses of the three case studies are similar to those of LHC point 5 of the study of Hinchliffe *et al.*[76], we adopt the same overall signal selection cuts which gave rise to only a small background contamination of mostly signal events: $\not{E}_T > max(100\text{ GeV}, 0.2M_{eff})$, at least four jets with $E_T > 50$ GeV, where the hardest jet has $E_T > 100$ GeV, transverse sphericity $S_T > 0.2$ and $M_{eff} > 800$ GeV.

In these events, we require at least two isolated leptons, and then plot the invariant mass of all same flavor/opposite sign dileptons. The results are shown in Fig. 12. In the case of the mSUGRA model, frame *a*), there is a sharp peak at $m(\ell^+\ell^-) \sim M_Z$, which comes from $\widetilde{Z}_2 \to \widetilde{Z}_1 Z^0$ decays where $\widetilde{Z}_2$ is produced in the gluino and squark cascade decays. In the case of MWDM1 in frame *b*), we again see a Z^0 peak, although here the Z^0s arise from $\widetilde{Z}_3$, $\widetilde{Z}_4$ and $\widetilde{W}_2$ decays. We also see the continuum distribution in $m(\ell^+\ell^-) < m_{\widetilde{Z}_2} - m_{\widetilde{Z}_1} = 31.9$ GeV. The cross section plotted here is ~ 0.05 pb, which would correspond to 5K events in 100 fb^{-1} of integrated luminosity (the sample shown in the figure contains just 406 events). In frame *c*)– with a cross section of ~ 0.05 pb (but just 267 actual entries)– we see again the Z^0 peak, but also we see again the $m(\ell^+\ell^-) < m_{\widetilde{Z}_2} - m_{\widetilde{Z}_1} = 22.9$ GeV continuum. In both these MWDM cases, the $m_{\widetilde{Z}_2} - m_{\widetilde{Z}_1}$ mass edge should be easily measurable. It should also be obvious that it is inconsistent with models based on gaugino mass unification, in that the projected ratios $M_1 : M_2 : M_3$ will not be in the order $1 :\sim 2 :\sim 7$ as in mSUGRA. Although the $\widetilde{Z}_2 - \widetilde{Z}_1$ mass edge will be directly measurable, the absolute neutralino and chargino masses will be difficult if not impossible to extract at the LHC.

In frame *d*), we show the spectrum from MHDM in the HB/FP region of the mSUGRA model. In this case, a $\widetilde{Z}_2 - \widetilde{Z}_1$ mass edge at 57.7 GeV should be visible. It will be accompanied by other continuum contributions, since in the case of MHDM with a small μ parameter, the $\widetilde{Z}_3$, $\widetilde{Z}_4$ and $\widetilde{W}_2$ should all be relatively light as well.

4.2 Linear e^+e^- collider

At a $\sqrt{s} = 500$ GeV ILC, the new physics reactions for the four case studies shown in Table 1 would include Zh, $\widetilde{W}_1^+\widetilde{W}_1^-$, $\widetilde{Z}_1\widetilde{Z}_2$ and $\widetilde{Z}_2\widetilde{Z}_2$ production. It was shown in Ref. [77] that, in the case of a small $\widetilde{W}_1 - \widetilde{Z}_1$ mass gap, chargino pair production events could still be identified above SM backgrounds. The chargino and neutralino masses can be inferred from the resultant dijet distribution in $\widetilde{W}_1^+\widetilde{W}_1^- \to (\bar{\ell}\nu_\ell\widetilde{Z}_1) + (q\bar{q}\widetilde{Z}_1)$ events[78, 79, 77]. Alternatively, the chargino mass may be extracted from threshold cross section measurements when the CM energy of the accelerator is tuned to operate just above $e^+e^- \to \widetilde{W}_1^+\widetilde{W}_1^-$ threshold. These measurements should allow the absolute mass scale of the sparticles to be pinned down, and will complement the $\widetilde{Z}_2 - \widetilde{Z}_1$ mass gap measurement from the CERN LHC. The combination of $m_{\widetilde{Z}_2}$, $m_{\widetilde{W}_1}$, $m_{\widetilde{Z}_1}$ and $m_{\widetilde{Z}_2} - m_{\widetilde{Z}_1}$ measurements will point to whether or not gaugino mass unification is realized in nature.

In addition, the $\widetilde{W}_1^+\widetilde{W}_1^-$, $\widetilde{Z}_1\widetilde{Z}_2$ and $\widetilde{Z}_2\widetilde{Z}_2$ production cross sections can all be measured as a function of beam polarization at the ILC. In the mSUGRA model, since $\widetilde{W}_1$ and $\widetilde{Z}_2$ are mainly wino-like, they will be produced at high rates for left-polarized electron beams, but at low rates for right-polarized beams[79]. The $\widetilde{Z}_1\widetilde{Z}_2$ production cross section also has a significant rise to it as beam polarization parameter $P_L(e^-)$ is increased from -1 to +1. These cross sections are plotted in frame *a*) of Fig. 13. In frame *b*), we show the same cross sections, except this time for the case of MWDM1. The $\widetilde{W}_1$ is still mainly wino-like, and so has a steeply rising cross section as $P_L(e^-)$ is increased. However, in this case $\widetilde{Z}_1$ and $\widetilde{Z}_2$ both have non-negligible bino components, which enhances their couplings to right-polarized electrons. Thus, $\sigma(e^+e^- \to \widetilde{Z}_1\widetilde{Z}_2)$ in the case of MWDM is a falling

distribution *vs.* $P_L(e^-)$. This is in fact borne out in frame *b*), and would be a strong signal for MWDM! In frame *c*), we plot the corresponding cross sections for the case of MWDM2. Again, $\widetilde{Z}_1\widetilde{Z}_2$ has a (slightly) falling cross section versus $P_L(e^-)$, indicating once again the presence of MWDM. In frame *d*), we show the corresponding cross sections for the case of MHDM. In this case, numerous other reactions such as $\widetilde{W}_1^+\widetilde{W}_2^-$, $\widetilde{Z}_1\widetilde{Z}_3$ and $\widetilde{Z}_2\widetilde{Z}_3$ should likely be kinematically accessible, and their presence will help serve to distinguish MHDM from MWDM.

While a combination of mass measurements at LHC and ILC would help to pin down the properties of MWDM, it is worth considering whether the case of MWDM can be confused with the case of MHDM, such as occurs in the HB/FP region of the mSUGRA model, or in models with non-universal Higgs masses[19, 17]. To answer this, we plot in Fig. 14 the $\widetilde{Z}_2-\widetilde{Z}_1$ mas gap versus $m_{\widetilde{W}_1}$ for MWDM scenarios which yield $\Omega_{\widetilde{Z}_1}h^2=0.11$, against mSUGRA models in the HB/FP region which also give $\Omega_{\widetilde{Z}_1}h^2=0.11$. We see that the MWDM points can span the entire range of $m_{\widetilde{W}_1}$ values shown, but that their $\widetilde{Z}_2-\widetilde{Z}_1$ mass gap is generally of order 15-40 GeV. Models with higher mass gaps are usually due to an overlap of MWDM with stau co-annihilation or A-funnel annihilation. The general trend for $m_{\widetilde{Z}_2}-m_{\widetilde{Z}_1}$ in the MWDM scenario is dictated by the interplay of wino coannihilations and of the growing wino component, both functions of the mass gap, which suppress $\Omega_{\widetilde{Z}_1}h^2$ to the required level. In contrast, the $\widetilde{Z}_2-\widetilde{Z}_1$ mass gap associated with MHDM in the HB/FP region is generally or order 40-80 GeV, at least until very large values of $m_{\widetilde{W}_1}\gtrsim 600$ GeV are generated. The largest mass gaps appear beyond the top quark mass threshold, whose effect is greatly enhanced, with respect to the MWDM case, due to Z and Higgs s-channel exchanges. At larger neutralino masses, the $\widetilde{Z}_2-\widetilde{Z}_1$ mass gap for MHDM shrinks to lower values, since a larger and larger higgsino fraction and stronger neutralino/chargino coannihilations are needed to fulfill the WMAP bound. Eventually, a pure higgsino LSP (with $m_{\widetilde{Z}_2}-m_{\widetilde{Z}_1}$ of the orders of few GeV) is needed to give $\Omega_{\widetilde{Z}_1}h^2=0.11$, at $m_{\widetilde{Z}_1}\sim 1$ TeV. For $m_{\widetilde{W}_1}\sim 600-800$ GeV, the MWDM and MHDM $\widetilde{Z}_2-\widetilde{Z}_1$ mass gaps overlap. In the large mass case, however, the two scenarios could still be differentiated by the remaining sparticle mass spectrum (*e.g.* $\widetilde{Z}_3$ would be light in the case of MHDM and heavy in the case of MWDM) and by the dependences of cross sections on electron beam polarization (if an energetic enough e^+e^- collider is built!).

5. Conclusions

In this paper, we have considered the phenomenological consequences of mixed wino dark matter. MWDM occurs in models with gaugino mass non-universality. MWDM may be obtained by modifying the paradigm mSUGRA model by either increasing the GUT scale value of M_1 or by decreasing M_2 until a sufficiently wino-like LSP is obtained as to fulfill the WMAP measured value of $\Omega_{CDM}h^2\sim 0.11$. If DM in nature is indeed composed of MWDM, then a number of consequences occur. In the sparticle mass spectrum, the $\widetilde{Z}_2-\widetilde{Z}_1$ and $\widetilde{W}_1-\widetilde{Z}_1$ mass gaps are expected to be reduced compared to what is expected in models with gaugino mass unification and a large μ parameter. Also, left- and right- sleptons are expected to be more nearly mass degenerate.

If MWDM comprises the dark matter of the universe, then both direct and indirect dark matter detection rates are expected to be enhanced compared to expectations from the mSUGRA model. However, to really pinpoint the existence of a partially wino-like $\widetilde{Z}_1$, collider experiments will be needed. The CERN LHC should be able to measure approximately the value of $m_{\tilde{g}}$, and in MWDM scenarios, also the $\widetilde{Z}_2 - \widetilde{Z}_1$ mass gap from the dilepton spectrum from $\widetilde{Z}_2 \to \ell\bar{\ell}\widetilde{Z}_1$ decay. These measurements should be enough to establish whether gaugino mass unification holds. Ultimately, a linear e^+e^- collider, the ILC, operating above $\widetilde{W}_1^+\widetilde{W}_1^-$ and $\widetilde{Z}_1\widetilde{Z}_2$ thresholds will be needed. The ILC should be able to measure the absolute $\widetilde{W}_1$, $\widetilde{Z}_1$ and $\widetilde{Z}_2$ masses. The dependence of the associated production cross sections on the electron beam polarization will point conclusively to the existence of MWDM.

Acknowledgments

We thank J. O'Farrill and X. Tata for conversations. This research was supported in part by the U.S. Department of Energy under contract number DE-FG02-97ER41022.

References

[1] H. Goldberg, *Phys. Rev. Lett.* **50** (1419) 1983; J. Ellis, J. Hagelin, D. Nanopoulos and M. Srednicki, Phys. Lett. **B127**, 233 (1983); J. Ellis, J. Hagelin, D. Nanopoulos, K. Olive and M. Srednicki, Nucl. Phys. **B238**, 453 (1984).

[2] Some recent papers include J. Feng, S. Su and F. Takayama, *Phys. Rev.* **D 70** (2004) 075019; J. Ellis, K. Olive, Y. Santoso and V. Spanos, *Phys. Lett.* **B 588** (2004) 7.

[3] For recent reviews, see *e.g.* C. Jungman, M. Kamionkowski and K. Griest,*Phys. Rept.* **267** (195) 1996; A. Lahanas, N. Mavromatos and D. Nanopoulos, *Int. J. Mod. Phys.* **D 12** (2003) 1529; M. Drees, `hep-ph/0410113`; K. Olive, "Tasi Lectures on Astroparticle Physics", `astro-ph/0503065`.

[4] P. Gondolo, J. Edsjo, P. Ullio, L. Bergstrom, M. Schelke and E. A. Baltz, JCAP **0407**, 008 (2004); G. Belanger, F. Boudjema, A. Pukhov and A. Semenov, `hep-ph/0405253`.

[5] IsaReD, by H. Baer, C. Balazs and A. Belyaev, *J. High Energy Phys.* **0203** (042) 2002.

[6] D. N. Spergel *et al.*, `astro-ph/0302209`; C. L. Bennett *et al.*, `astro-ph/0302207`.

[7] J. Ellis, K. Olive, Y. Santoso and V. Spanos, *Phys. Lett.* **B 565** (2003) 176; H. Baer and C. Balazs, JCAP**05** (2003) 006; U. Chattapadhyay, A. Corsetti and P. nath, *Phys. Rev.* **D 68** (2003) 035005; A. Lahanas and D. V. Nanopoulos, *Phys. Lett.* **B 568** (2003) 55.

[8] A. Chamseddine, R. Arnowitt and P. Nath, *Phys. Rev. Lett.* **49** (1982) 970; R. Barbieri, S. Ferrara and C. Savoy, *Phys. Lett.* **B 119** (1982) 343; N. Ohta, *Prog. Theor. Phys.* **70** (1983) 542; L. J. Hall, J. Lykken and S. Weinberg, *Phys. Rev.* **D 27** (1983) 2359; for reviews, see H. P. Nilles, *Phys. Rep.* **110** (1984) 1, and P. Nath, `hep-ph/0307123`.

[9] See *e.g.*, H. Baer and M. Brhlik, *Phys. Rev.* **D 53** (1996) 597.

[10] J. Ellis, T. Falk and K. Olive, *Phys. Lett.* **B 444** (1998) 367; J. Ellis, T. Falk, K. Olive and M. Srednicki, *Astropart. Phys.* **13** (2000) 181; M.E. Gómez, G. Lazarides and C. Pallis, *Phys. Rev.* **D 61** (2000) 123512 and *Phys. Lett.* **B 487** (2000) 313; R. Arnowitt, B. Dutta and Y. Santoso, *Nucl. Phys.* **B 606** (2001) 59; see also Ref. [5]

[11] K. L. Chan, U. Chattopadhyay and P. Nath, *Phys. Rev.* **D 58** (1998) 096004. J. Feng, K. Matchev and T. Moroi, *Phys. Rev. Lett.* **84** (2000) 2322 and *Phys. Rev.* **D 61** (2000) 075005; see also H. Baer, C. H. Chen, F. Paige and X. Tata, *Phys. Rev.* **D 52** (1995) 2746 and *Phys. Rev.* **D 53** (1996) 6241; H. Baer, C. H. Chen, M. Drees, F. Paige and X. Tata, *Phys. Rev.* **D 59** (1999) 055014;

[12] M. Drees and M. Nojiri, *Phys. Rev.* **D 47** (1993) 376; H. Baer and M. Brhlik, *Phys. Rev.* **D 57** (1998) 567 and Ref. [9]; H. Baer, M. Brhlik, M. Diaz, J. Ferrandis, P. Mercadante, P. Quintana and X. Tata, *Phys. Rev.* **D 63** (2001) 015007; J. Ellis, T. Falk, G. Ganis, K. Olive and M. Srednicki, *Phys. Lett.* **B 510** (2001) 236; L. Roszkowski, R. Ruiz de Austri and T. Nihei, *J. High Energy Phys.* **0108** (024) 2001. A. Lahanas and V. Spanos, *Eur. Phys. J.* **C 23** (2002) 185.

[13] R. Arnowitt and P. Nath, *Phys. Rev. Lett.* **70** (1993) 3696; H. Baer and M. Brhlik, Ref. citebulk; A. Djouadi, M. Drees and J. Kneur, `hep-ph/0504090`.

[14] C. Böhm, A. Djouadi and M. Drees, *Phys. Rev.* **D 30** (2000) 035012; J. R. Ellis, K. A. Olive and Y. Santoso, *Astropart. Phys.* **18** (2003) 395; J. Edsjö, *et al.*, JCAP **04** (2003) 001

[15] H. Baer, A. Belyaev, T. Krupovnickas and A. Mustafayev, *J. High Energy Phys.* **0406** (2004) 044.

[16] D. Auto, H. Baer, A. Belyaev and T. Krupovnickas, *J. High Energy Phys.* **0410** (2004) 066.

[17] H. Baer, A. Mustafayev, S. Profumo, A. Belyaev and X. Tata, `hep-ph/0412059` and `hep-ph/0504001`.

[18] S. Profumo, *Phys. Rev.* **D 68** (2003) 015006

[19] J. Ellis, K. Olive and Y. Santoso, *Phys. Lett.* **B 539** (2002) 107; J. Ellis, T. Falk, K. Olive and Y. Santoso, *Nucl. Phys.* **B 652** (2003) 259.

[20] M. Drees, `hep-ph/0410113`.

[21] H. Baer, M. Diaz, P. Quintana and X. Tata, *J. High Energy Phys.* **0004** (2000) 016.

[22] J. Amundsen *et al.*, `hep-ph/9609374`; G. Anderson, H. Baer, C. H. Chen and X. Tata, *Phys. Rev.* **D 61** (2000) 095005.

[23] N. Chamoun, C. S. Huang, C. Liu and X. Wu, *Nucl. Phys.* **B 624** (2002) 81.

[24] U. Chattapadhyay, A. Corsetti and P. Nath, *Phys. Rev.* **D 66** (2002) 035003.

[25] A. Brignole, L. E. Ibanez and C. Munoz, *Nucl. Phys.* **B 422** (1994) 125 [Erratum-ibid. B **436** (1995) 747]; . Brignole, L. E. Ibanez, C. Munoz and C. Scheich, *Z. Physik* **C 74** (1997) 157.

[26] R. Dermisek and A. Mafi, *Phys. Rev.* **D 65** (2002) 055002; H. Baer, C. Balazs, A. Belyaev, R. Dermisek, A. Mafi and A. Mustafayev, *J. High Energy Phys.* **0205** (2002) 061.

[27] L. Randall and R. Sundrum, *Nucl. Phys.* **B 557** (1999) 79; G. Giudice, M. Luty, H. Murayama and R. Rattazzi, *J. High Energy Phys.* **9812** (1998) 27.

[28] T. Moroi and L. Randall, *Nucl. Phys.* **B 570** (2000) 455.

[29] K. Griest and L. Roszkowski, *Phys. Rev.* **D 46** (1992) 3309.

[30] A. Corsetti and P. Nath, *Phys. Rev.* **D 64** (2001) 125010.

[31] A. Birkedal-Hansen and B. Nelson, *Phys. Rev.* **D 64** (2001) 015008 and *Phys. Rev.* **D 67** (2003) 095006.

[32] V. Bertin, E. Nezri and J. Orloff, *J. High Energy Phys.* **0302** (2003) 046.

[33] A. Bottino, F. Donato, N. Fornengo and S. Scopel, *Phys. Rev.* **D 70** (2004) 015005.

[34] G. Belanger, F. Boudjema, A. Cottrant, A. Pukhov and A. Semenov, *Nucl. Phys.* **B 706** (2005) 411.

[35] D. Cerdeno and C. Munoz, *J. High Energy Phys.* **0410** (2004) 015; Y. Mambrini and C. Munoz, JCAP **0410** (2004) 003; see also S. Baek, D. Cerdeno, Y. G. Kim, P. Ko and C. Munoz, `hep-ph/0505019`.

[36] A. Masiero, S. Profumo and P. Ullio, *Nucl. Phys.* **B 712** (2005) 86.

[37] H. Baer, A. Mustafayev, E. Park, S. Profumo and X. Tata, in preparation.

[38] ISAJET v7.69, by H. Baer, F. Paige, S. Protopopescu and X. Tata, `hep-ph/0312045`.

[39] P. Gondolo and G. Gelmini, *Nucl. Phys.* **B 360** (1991) 145; J. Edsjo and P. Gondolo, *Phys. Rev.* **D 56** (1997) 1879.

[40] H. Baer and X. Tata, *Weak Scale Supersymmetry: From Superfields to Scattering Events*, (Cambridge University Press, January, 2006).

[41] For a review, see *e.g.* G. Eigen, R. Gaitskell, G. Kribs and K. Matchev, `hep-ph/0112312`; see also D. Hooper and L. T. Wang, *Phys. Rev.* **D 69** (2004) 035001; W. de Boer, M. Herold, C. Sander and V. Zhukov, `hep-ph/0309029`.

[42] J. Feng, K. Matchev and F. Wilczek, *Phys. Lett.* **B 482** (2000) 388 and *Phys. Rev.* **D 63** (2001) 045024.

[43] P. Gondolo, J. Edsjo, P. Ullio, L. Bergstrom, M. Schelke and E. A. Baltz, `astro-ph/0211238`.

[44] J.F. Navarro et al., Mon. Not. Roy. Astron. Soc. **349** (2004) 1039, `astro-ph/0311231`; the adiabatic contraction of the halo follows Blumental et al., *Astrophys. J.* **301** (1986) 27. For the halo parameter choices see also ref. [47].

[45] H. Baer and J. O'Farrill, JCAP**03**, 012 (2004).

[46] H. Baer, A. Belyaev, T. Krupovnickas and J. O'Farrill, JCAP **0404** (2004) 005.

[47] S. Profumo and P. Ullio, JCAP **0407** (2004) 006.

[48] For a recent analysis, see H. Baer, C. Balazs, A. Belyaev and J. O'Farrill, JCAP**0309**, 2003 (007); a subset of earlier work includes M. Goodman and E. Witten, *Phys. Rev.* **D 31** (1985) 3059; K. Griest, *Phys. Rev. Lett.* **61** (1988) 666 and *Phys. Rev.* **D 38** (1988) 2357 [Erratum-ibid. D **39**, 3802 (1989)]; M. Drees and M. Nojiri, *Phys. Rev.* **D 47** (1993) 4226 and *Phys. Rev.* **D 48** (1993) 3483; V. A. Bednyakov, H. V. Klapdor-Kleingrothaus and S. Kovalenko, *Phys. Rev.* **D 50** (1994) 7128; P. Nath and R. Arnowitt, *Phys. Rev. Lett.* **74** (1995) 4592; L. Bergstrom and P. Gondolo, *Astropart. Phys.* **5** (1996) 263; H. Baer and M. Brhlik, *Phys. Rev.* **D 57** (1998) 567; J. Ellis, A. Ferstl and K. Olive, *Phys. Lett.* **B 481** (2000) 304 and *Phys. Rev.* **D 63** (2001) 065016; E. Accomando, R. Arnowitt, B. Dutta and Y. Santoso, *Nucl. Phys.* **B 585** (2000) 124; A. Bottino, F. Donato, N. Fornengo and S. Scopel, *Phys. Rev.* **D 63** (2001) 125003; M. E. Gomez and J. D. Vergados, *Phys. Lett.* **B 512** (2001) 252; A. B. Lahanas, D. V. Nanopoulos and V. C. Spanos, *Phys. Lett.* **B 518** (2001) 94; A. Corsetti and P. Nath, *Phys. Rev.* **D 64** (2001) 115009; E. A. Baltz and P. Gondolo, *Phys. Rev. Lett.* **86** (2001) 5004; M. Drees, Y. G. Kim, T. Kobayashi and M. M. Nojiri, *Phys. Rev.* **D 63** (2001) 115009; see also J. Feng, K. Matchev and F. Wilczek,

Ref. [42]; . R. Ellis, A. Ferstl, K. A. Olive and Y. Santoso, *Phys. Rev.* **D 67** (2003) 123502; J. R. Ellis, K. A. Olive, Y. Santoso and V. C. Spanos, *Phys. Rev.* **D 69** (2004) 015005; see C. Munoz, `hep-ph/0309346` for a recent review.

[49] See H. Baer, C. Balazs, A. Belyaev and J. O'Farrill, Ref. [48]

[50] D. S. Akerib *et al.* (CDMS Collaboration), `astro-ph/0405033` (2004).

[51] A. Benoit *et al.* (Edelweiss Collaboration), *Phys. Lett.* **B 545** (2002) 43.

[52] M. Bravin *et al.* (CRESST Collaboration), *Astrophys. J.* **12** (1999) 107.

[53] N. Spooner *et al.* (Zeplin-1Collaboration), in *Proc. of the APS/DPF/DPB Summer Study on the Future of Particle Physics (Snowmass 2001)* ed. N. Graf, eConf **C010630**, E601 (2001).

[54] Y. Suzuki *et al.* (Xenon Colaboration), `hep-ph/0008296`.

[55] H. V. Klapdor-Kleingrothaus, A. Dietz and I. V. Krivosheina, *Nucl. Phys.* **124** *(Proc. Suppl.)* (2003) 209.

[56] D. B. Cline *et al.* (ZEPLIN-4 Collaboration), *Nucl. Phys.* **124** *(Proc. Suppl.)* (2003) 229.

[57] See talk by C. Rubbia at 6th UCLA Symposium on *Sources and Detection of Dark Matter and Dark Energy in the Universe*, Marina del Ray, CA, February (2004).

[58] J. Silk, K. Olive and M. Srednicki, *Phys. Rev. Lett.* **55** (1985) 257; K. Freese, *Phys. Lett.* **B 167** (1986) 295; L. Krauss, M. Srednicki and F. Wilczek, *Phys. Rev.* **D 33** (1986) 2079; V. Berezinsky, A. Bottino, J. R. Ellis, N. Fornengo, G. Mignola and S. Scopel, *Astropart. Phys.* **5** (1996) 333; L. Bergstrom, J. Edsjo and P. Gondolo, *Phys. Rev.* **D 55** (1997) 1765 and *Phys. Rev.* **D 58** (1998) 103519; A. Bottino, F. Donato, N. Fornengo and S. Scopel, *Astropart. Phys.* **10** (1999) 203; A. Corsetti and P. Nath, *Int. J. Mod. Phys.* **A 15** (2000) 905; V. Barger, F. Halzen, D. Hooper and C. Kao, *Phys. Rev.* **D 65** (2002) 075022; V. Bertin, E. Nezri and J. Orloff, *Eur. Phys. J.* **C 26** (2002) 111 and *J. High Energy Phys.* **0302** (2003) 046.

[59] E. Carmona *et al.*, (Antares Collaboration), *Nucl. Phys.* **95** *(Proc. Suppl.)* (2001) 161.

[60] J. Ahrens *et al.*, (IceCube Collaboration), *Nucl. Phys.* **118** *(Proc. Suppl.)* (2003) 388; F. Halzen, `astro-ph/0311004`; F. Halzen and D. Hooper, JCAP**0401** (2004) 002.

[61] F. Stecker, *Phys. Lett.* **B 201** (1988) 529; F. W. Stecker and A. J. Tylka, *Astrophys. J.* **343** (1989) 169; S. Rudaz and F. Stecker, *Astrophys. J.* **368** (1991) 406; M. Urban *et al.*, *Phys. Lett.* **B 293** (1992) 149; V. Berezinsky, A. Gurevich and K. Zybin, *Phys. Lett.* **B 294** (1992) 221; V. Berezinsky, A. Bottino and G. Mignola, *Phys. Lett.* **B 325** (1994) 136; L. Bergstrom, P. Ullio and J. H. Buckley, *Astropart. Phys.* **9** (1998) 137; L. Bergstrom, J. Edsjö and P. Ullio, *Phys. Rev.* **D 58** (1998) 083507; J. Buckley *et al.*, `astro-ph/0201160`; P. Ullio, L. Bergstrom, J. Edsjö and C. Lacey, *Phys. Rev.* **D 66** (2002) 123502.

[62] H. A. Mayer-Hasselwander *et al.* (EGRET Collaboration), MPE-440 (1998).

[63] A. Morselli *et al.*, (GLAST Collaboration), *Nucl. Phys.* **113** *(Proc. Suppl.)* (2002) 213.

[64] S. Rudaz and F. Stecker, *Astrophys. J.* **325** (1988) 16; A. Tylka, *Phys. Rev. Lett.* **63** (1989) 840; M. Turner and F. Wilczek, *Phys. Rev.* **D 42** (1990) 1001; M. Kamionkowski and M. Turner, *Phys. Rev.* **D 43** (1991) 1774; A. Moskalenko and A. Strong, *Phys. Rev.* **D 60** (1999) 063003; E. Baltz and J. Edsjö, *Phys. Rev.* **D 59** (1999) 023511; G. Kane, L. T. Wang and J. Wells, *Phys. Rev.* **D 65** (2002) 057701; E. Baltz, J. Edsjo, K. Freese and P. Gondolo, *Phys. Rev.* **D 65** (2002) 063511; G. Kane, L. T. Wang and T. Wang, *Phys. Lett.* **B 536** (2002) 263; D. Hooper, J. Taylor and J. Silk, `hep-ph/0312076`.

[65] M. A. DuVernois *et al.* (HEAT Collaboration), *Astrophys. J.* **559** (2001) 296.

[66] M. Pearce (Pamela Collaboration), *Nucl. Phys.* **113** *(Proc. Suppl.)* (2002) 314.

[67] J. Casaus *et al.* (AMS Collaboration), *Nucl. Phys.* **114** *(Proc. Suppl.)* (2003) 259.

[68] F. Stecker, S. Rudaz and T. Walsh, *Phys. Rev. Lett.* **55** (1985) 2622; F. Stecker and A. J. Tylka, *Astrophys. J.* **336** (1989) L51; P. Chardonnet, Mignola, P. Salati and R. Taillet, *Phys. Lett.* **B 384** (1996) 161; A. Bottino, F. Donato, N. Fornengo and P. Salati, *Phys. Rev.* **D 58** (1998) 123503; L. Bergstrom, J. Edsjo and P. Ullio, *Astrophys. J.* **526** (1999) 215.

[69] S. Orito *et al.* (BESS Collaboration), *Phys. Rev. Lett.* **84** (2000) 1078.

[70] H. Fuke *et al.* (BESS Collaboration), `astro-ph/0504361`.

[71] K. Mori, C. J. Hailey, E. A. Baltz, W. W. Craig, M. Kamionkowski, W. T. Serber and P. Ullio, *Astrophys. J.* **566** (2002) 604.

[72] S. Profumo and C.E. Yaguna, *Phys. Rev.* **D 70** (2004) 095004

[73] H. Baer, J. Ellis, G. Gelmini, D. V. Nanopoulos and X. Tata, *Phys. Lett.* **B 161** (1985) 175; G. Gamberini, *Z. Physik* **C 30** (1986) 605; H. Baer, V. Barger, D. Karatas and X. Tata, *Phys. Rev.* **D 36** (1987) 96; H. Baer, X. Tata and J. Woodside, *Phys. Rev.* **D 45** (1992) 142.

[74] H. Baer, K. Hagiwara and X. Tata, *Phys. Rev.* **D 35** (1987) 1598; H. Baer, D. Dzialo-Karatas and X. Tata, *Phys. Rev.* **D 42** (1990) 2259; H. Baer, C. Kao and X. Tata, *Phys. Rev.* **D 48** (1993) 5175; H. Baer, C. H. Chen, F. Paige and X. Tata, *Phys. Rev.* **D 50** (1994) 4508; see also ref. [76].

[75] H. Baer, C. Balazs, A. Belyaev, T. Krupovnickas and X. Tata, *J. High Energy Phys.* **0306** (2003) 054. For earlier work, see H. Baer, C. H. Chen, F. Paige and X. Tata, *Phys. Rev.* **D 52** (1995) 2746 and *Phys. Rev.* **D 53** (1996) 6241; H. Baer, C. H. Chen, M. Drees, F. Paige and X. Tata, *Phys. Rev.* **D 59** (1999) 055014; S. Abdullin and F. Charles, *Nucl. Phys.* **B 547** (1999) 60; S. Abdullin *et al.* (CMS Collaboration), `hep-ph/9806366`; B. Allanach, J. Hetherington, A. Parker and B. Webber, *J. High Energy Phys.* **08** (2000) 017.

[76] I. Hinchliffe *et al.*, *Phys. Rev.* **D 55** (1997) 5520 and *Phys. Rev.* **D 60** (1999) 095002; H. Bachacou, I. Hinchliffe and F. Paige, *Phys. Rev.* **D 62** (2000) 015009; Atlas Collaboration, LHCC 99-14/15.

[77] H. Baer, A. Belyaev, T. Krupovnickas and X. Tata, *J. High Energy Phys.* **0402** (2004) 007; H. Baer, T. Krupovnickas and X. Tata, *J. High Energy Phys.* **0406** (2004) 061.

[78] T. Tsukamoto, K. Fujii, H. Murayama, M. Yamaguchi and Y. Okada, *Phys. Rev.* **D 3153** (1995) 3153.

[79] H. Baer, R. Munroe and X. Tata, *Phys. Rev.* **D 54** (1996) 6735.

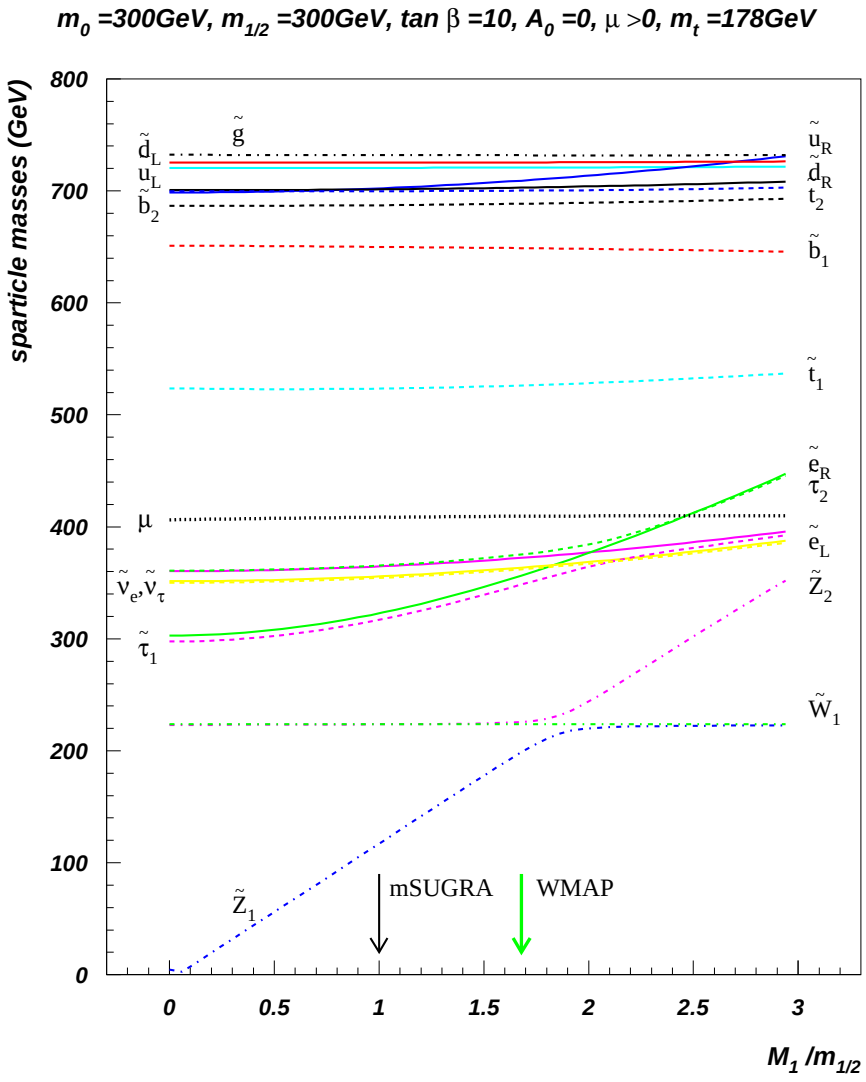

Figure 3: A plot of various sparticle masses *vs.* $M_1/m_{1/2}$ for $m_0 = 300$ GeV, $m_{1/2} = 300$ GeV, $A_0 = 0$, $\tan\beta = 10$ and $\mu > 0$.

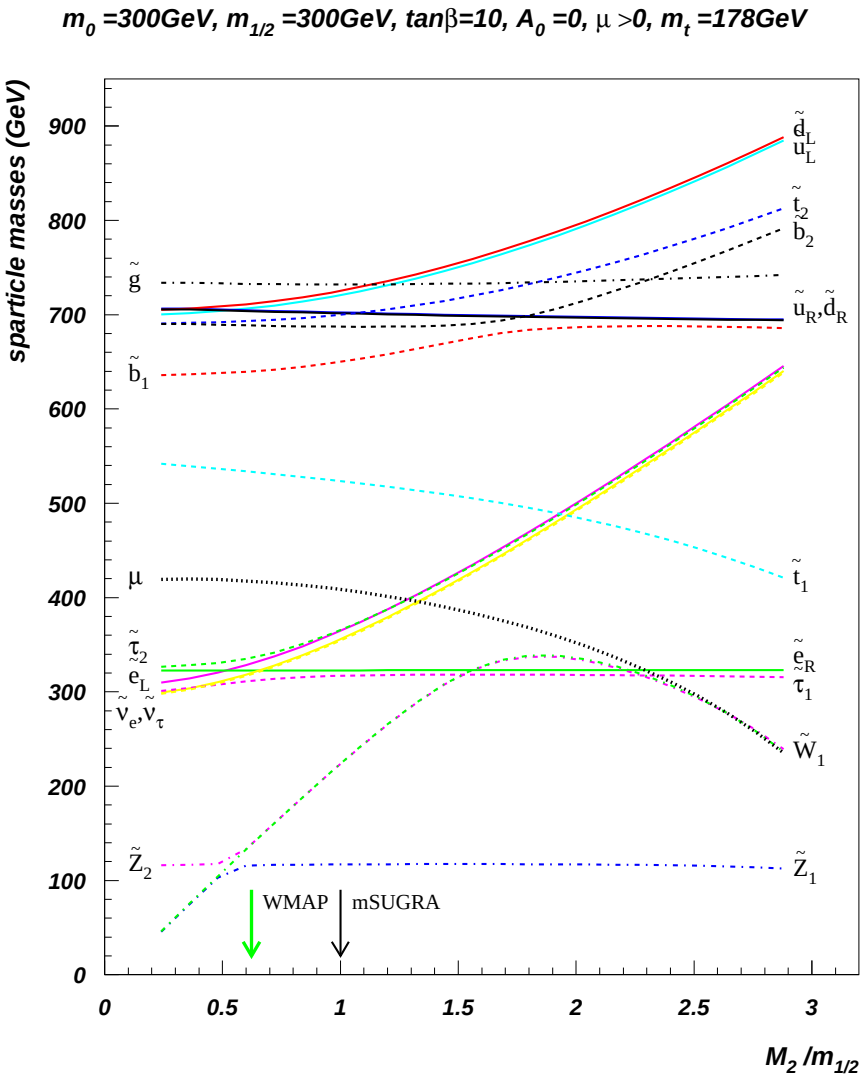

Figure 4: A plot of various sparticle masses *vs.* $M_2/m_{1/2}$ for $m_0 = 300$ GeV, $m_{1/2} = 300$ GeV, $A_0 = 0$, $\tan\beta = 10$ and $\mu > 0$.

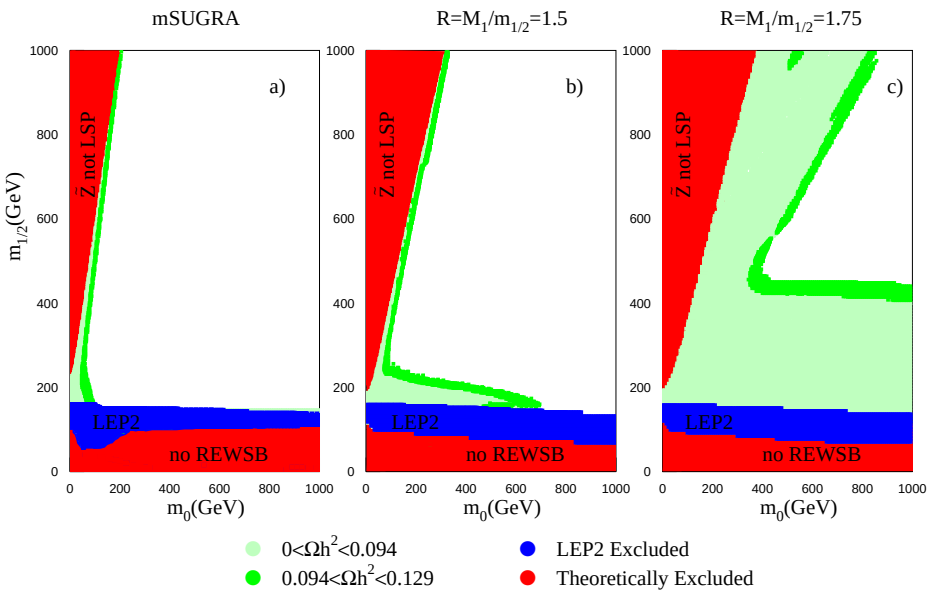

Figure 5: WMAP allowed regions in the m_0 *vs.* $m_{1/2}$ plane for $\tan\beta = 10$, $A_0 = 0$, $\mu > 0$ and *a)* $M_1/m_{1/2} = 1$, *b)* $M_1/m_{1/2} = 1.5$ and *c)* $M_1/m_{1/2} = 1.75$.

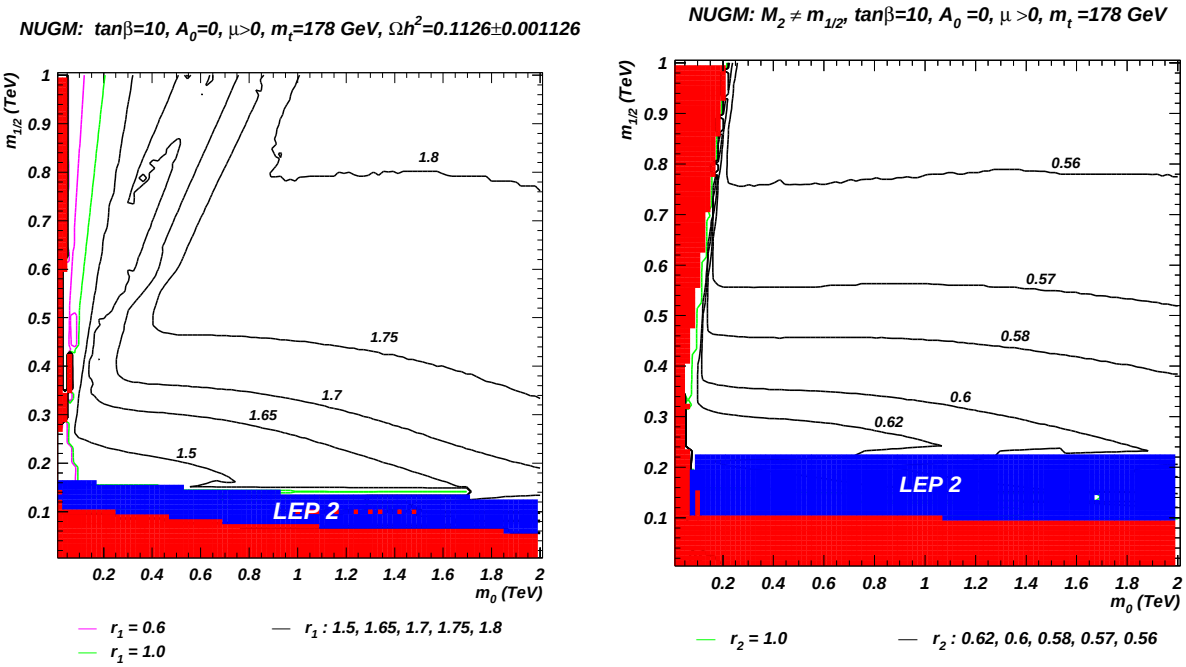

Figure 6: Contours of *a)* r_1 and *b)* r_2 in the m_0 *vs.* $m_{1/2}$ plane for $\tan\beta = 10$, $A_0 = 0$, $\mu > 0$. Each point has $\Omega_{\tilde{Z}_1} h^2 = 0.11$.

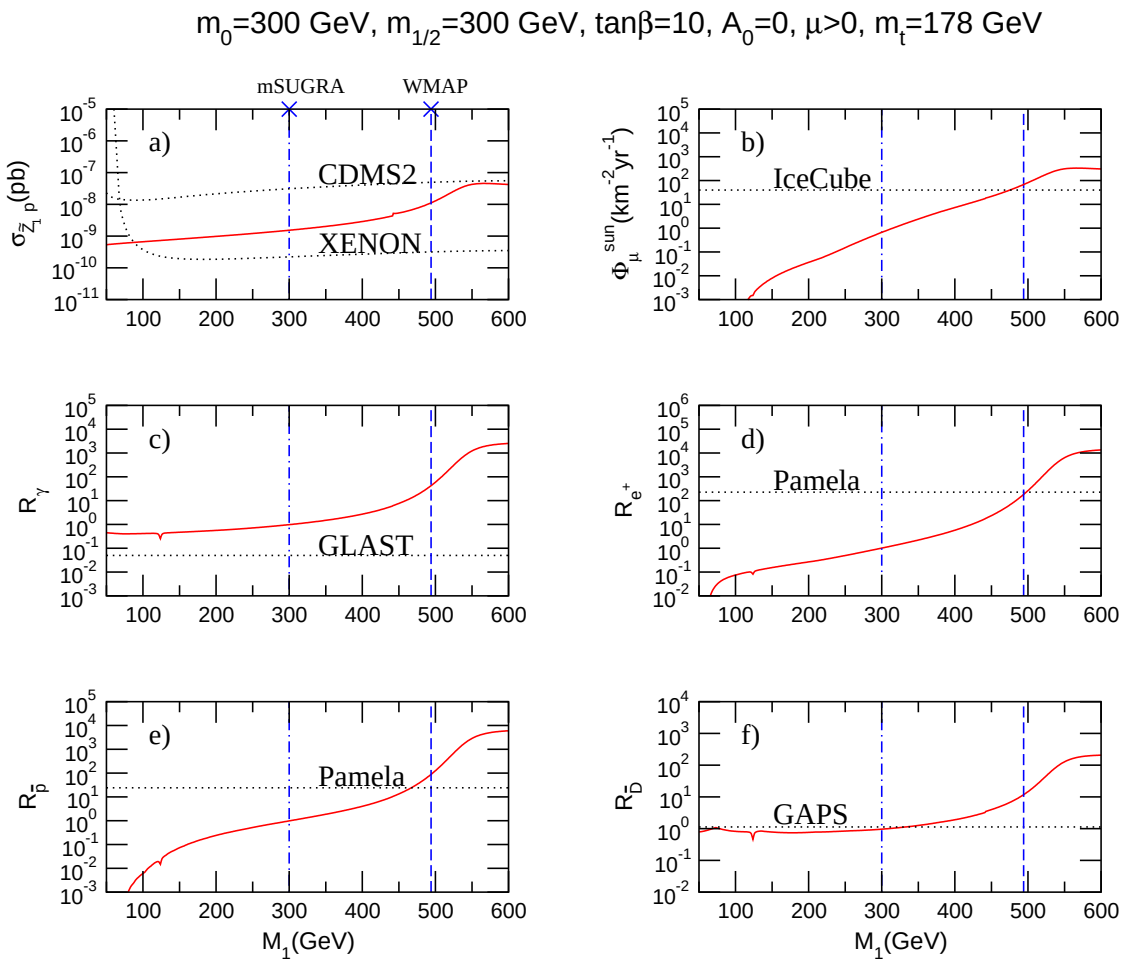

Figure 7: Rates for direct and indirect detection of neutralino dark matter vs. M_1 for $m_0 = m_{1/2} = 300$ GeV, with $\tan\beta = 10$, $A_0 = 0$, $\mu > 0$. Frames *c*) -*f*) show the ratio of indirect detection rates compared to the mSUGRA model. In this plot, we adopt the N03 distribution for halo dark matter.

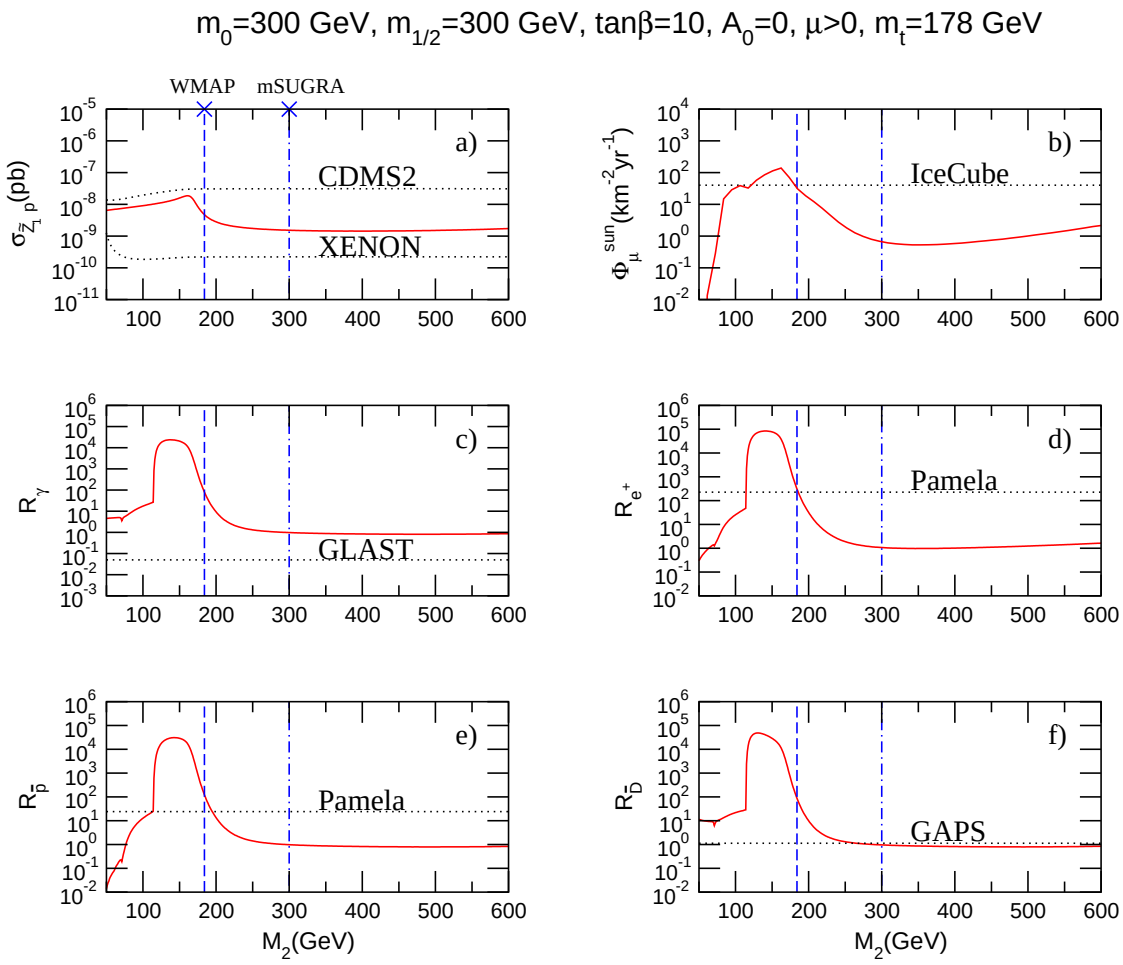

Figure 8: Rates for direct and indirect detection of neutralino dark matter vs. M_2 for $m_0 = m_{1/2} = 300$ GeV, with $\tan\beta = 10$, $A_0 = 0$, $\mu > 0$. Frames *c*) -*f*) show the ratio of indirect detection rates compared to the mSUGRA model. In this plot, we adopt the N03 distribution for halo dark matter.

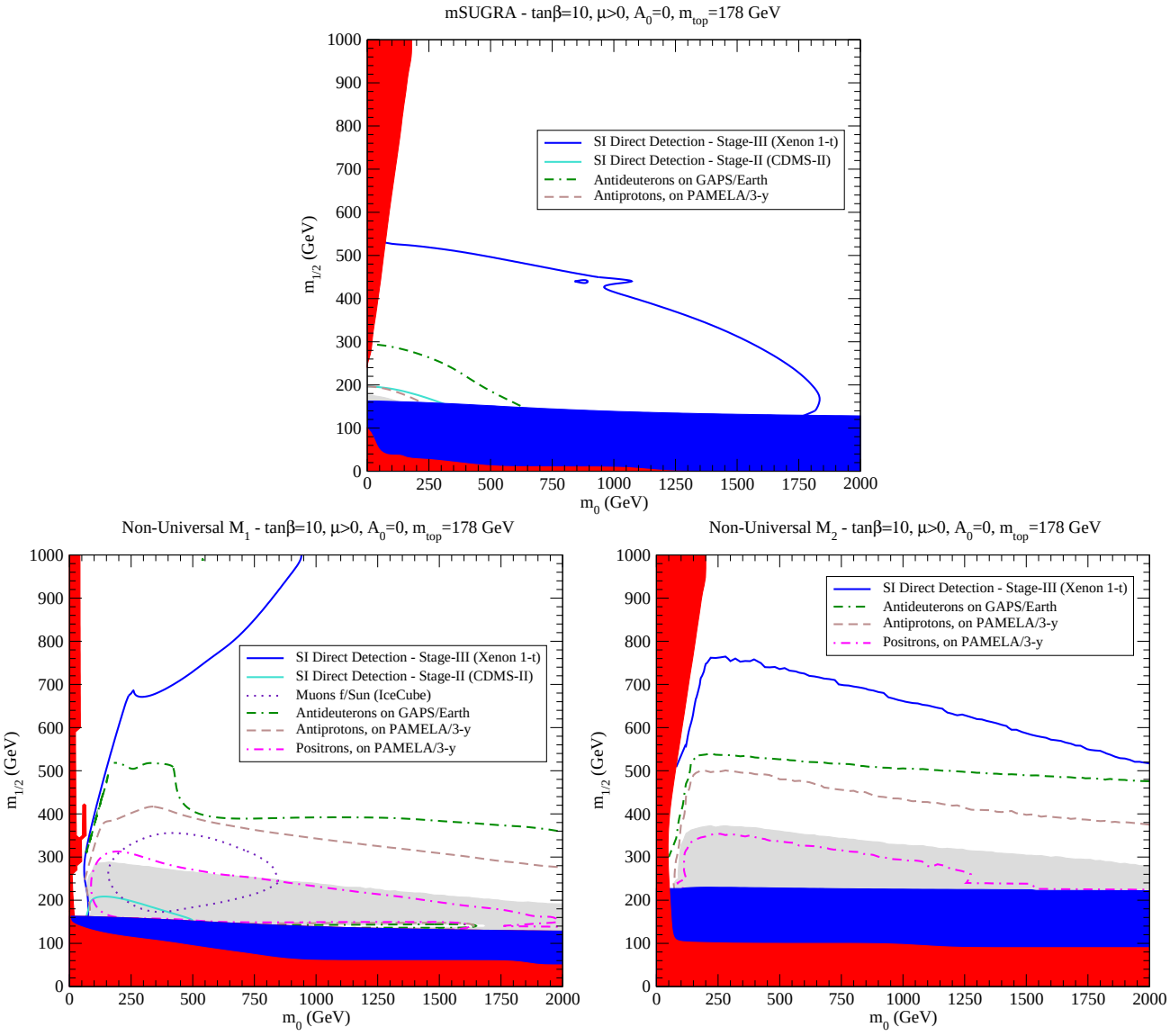

Figure 9: Regions of visibility for direct and indirect dark matter searches in the m_0 *vs.* $m_{1/2}$ plane for $\tan\beta = 10$, $A_0 = 0$, $\mu > 0$. The upper frame *a*) shows the mSUGRA model, while frame *b*) corresponds to the MWDM model with non-universal M_1 and frame *c*) with non-universal M_2. In this plot, we adopt the Adiabatically Contracted N03 Halo Model for the galactic dark matter distribution. For this halo model, detection of γs by GLAST should occur over all three planes.

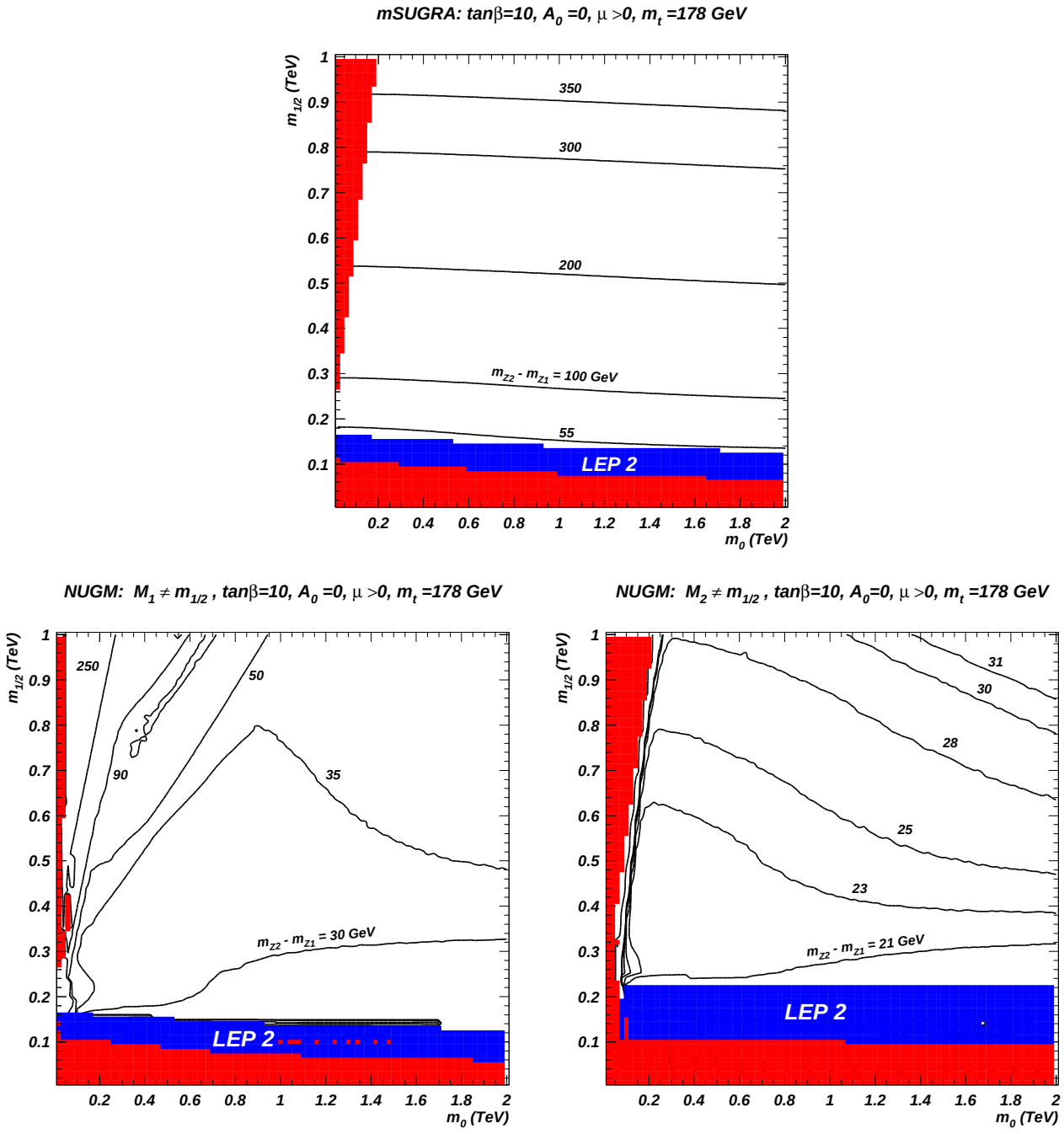

Figure 10: Contours of $m_{\tilde{Z}_2} - m_{\tilde{Z}_1}$ mass gap in the m_0 *vs.* $m_{1/2}$ plane for $\tan\beta = 10$, $A_0 = 0$, $\mu > 0$ and *a*) mSUGRA model, *b*) $M_1 > m_{1/2}$ MWDM and *c*) $M_2 < m_{1/2}$ MWDM.

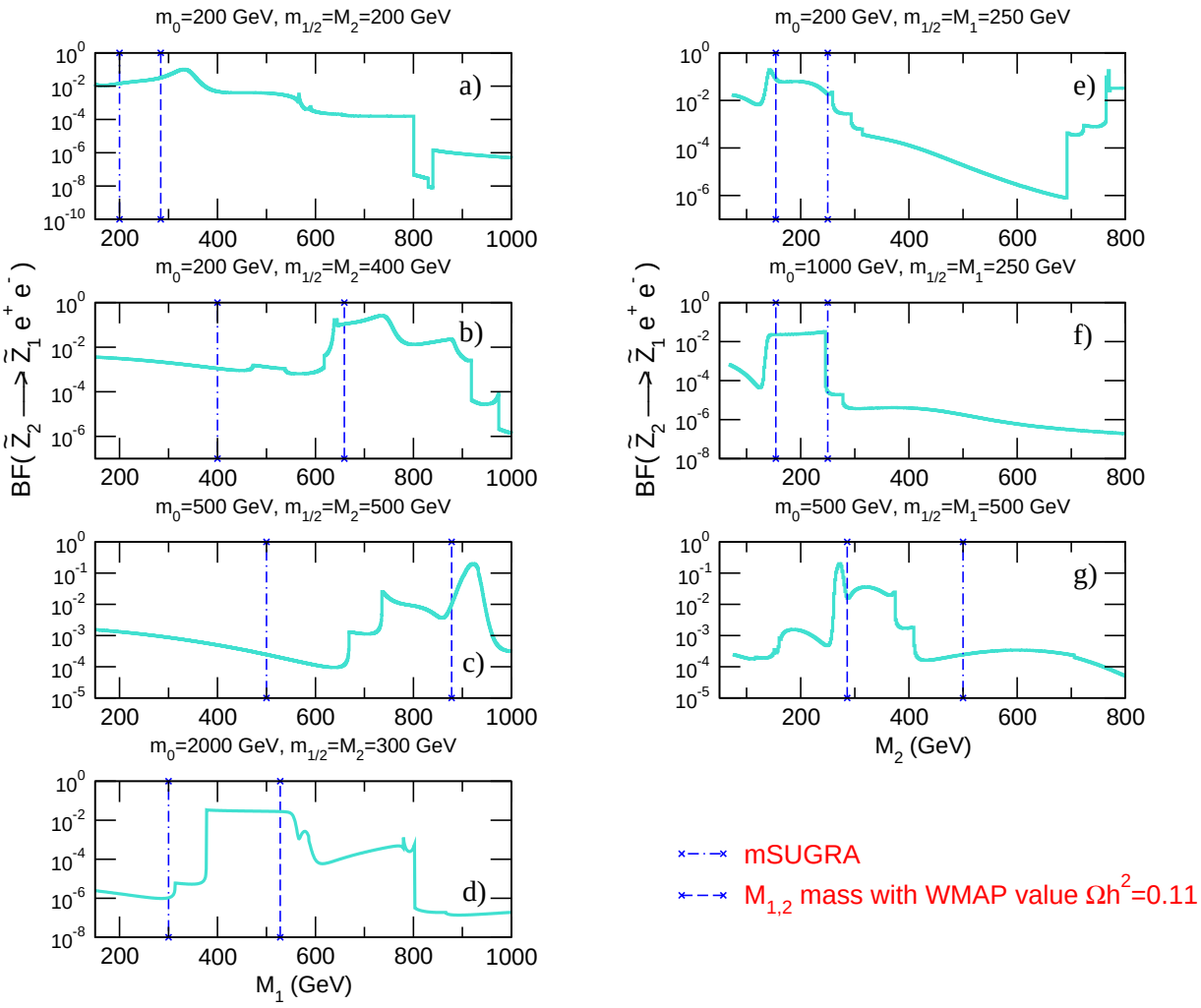

Figure 11: The branching fraction for $\widetilde{Z}_2 \to \widetilde{Z}_1 e^+ e^-$ decay is plotted vs. M_1 (left-side) or M_2 (right-side) for various points in the MWDM model parameter space. The $M_{1,2}$ value from mSUGRA is denoted by the dot-dashed lines, while the $M_{1,2}$ value which gives $\Omega_{\widetilde{Z}_1} h^2 = 0.11$ is indicated by dotted lines.

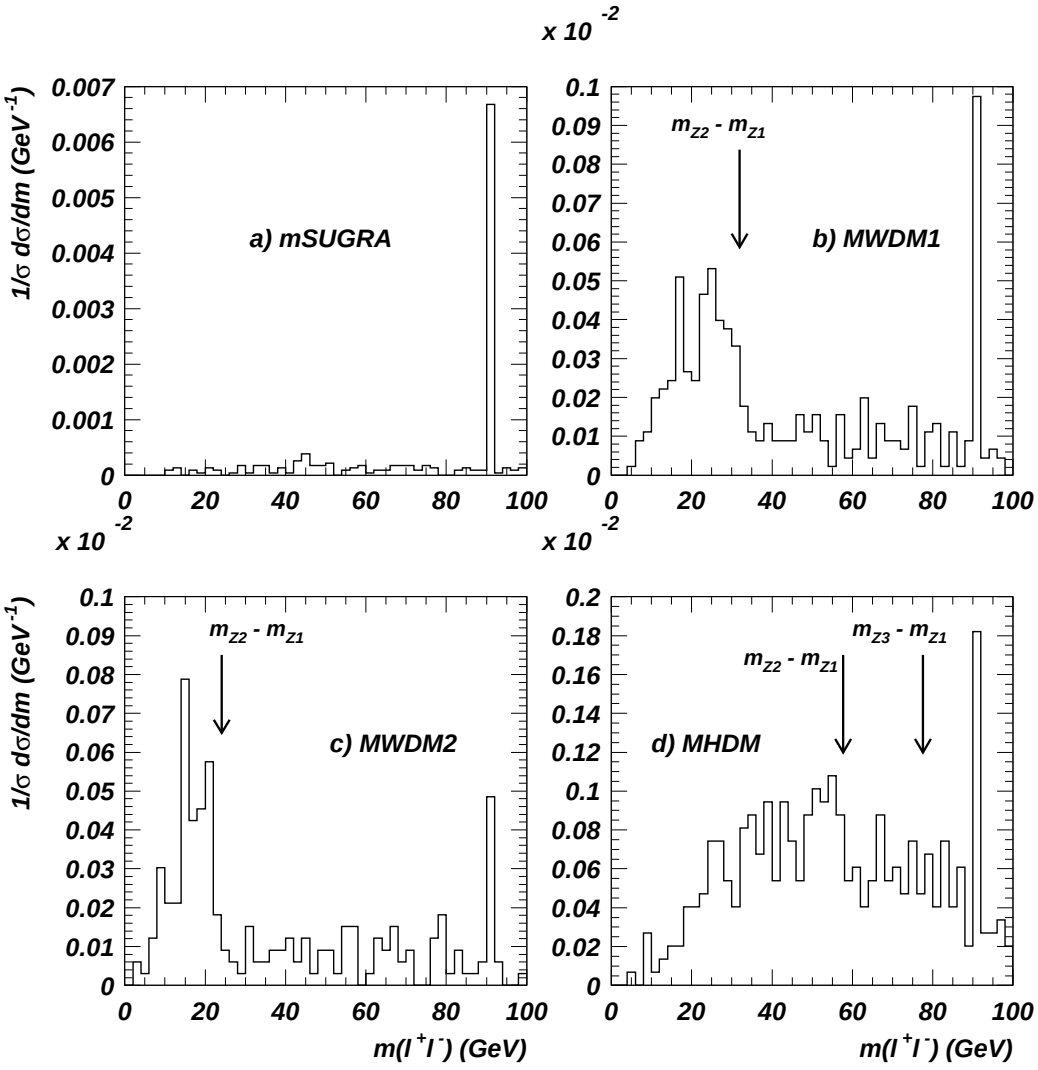

Figure 12: Distribution of same flavor/opposite sign dileptons from SUSY events at the CERN LHC from *a*) mSUGRA, *b*) MWDM1, *c*) MWDM2 and *d*) MHDM cases as in Table 1.

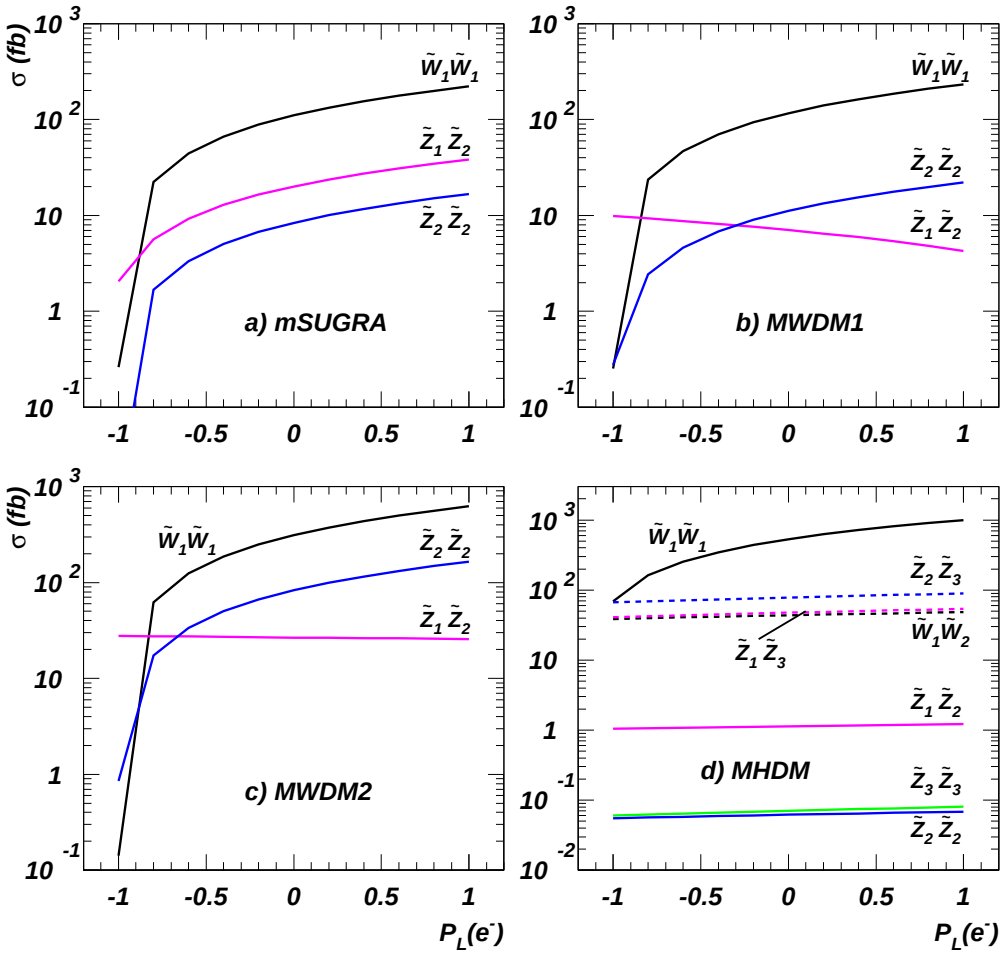

Figure 13: Plot of cross section for $e^+e^- \to \widetilde{W}_1^+\widetilde{W}_1^-$, $\widetilde{Z}_1\widetilde{Z}_2$ and $\widetilde{Z}_2\widetilde{Z}_2$ versus electron beam polarization $P_L(e^-)$ for a $\sqrt{s} = 500$ GeV ILC for *a*) mSUGRA, *b*) MWDM1, *c*) MWDM2 and *d*) MHDM with parameters as in table 1.

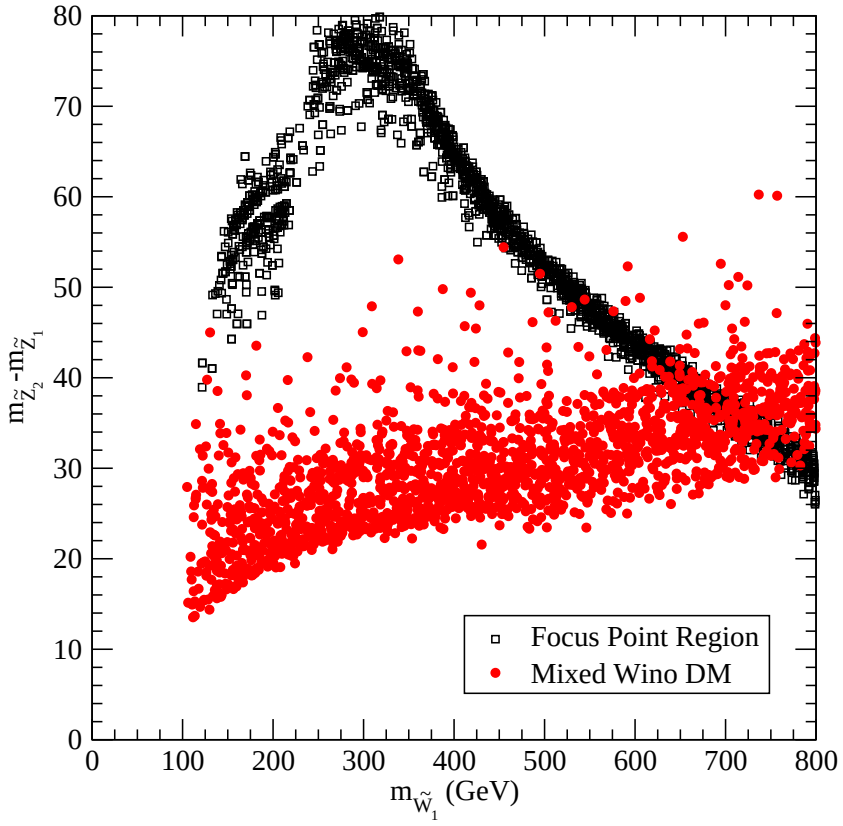

Figure 14: Correlation between $m_{\tilde{Z}_2} - m_{\tilde{Z}_1}$ and $m_{\widetilde{W}_1}$ in models with MWDM and MHDM in the HB/FP region.